

# Active Matter Physics

2025-04-10



# Table of contents

<b>1 Active Matter Physics</b>	<b>1</b>
<b>2 Active Matter: General Course Description</b>	<b>3</b>
2.1 Course Overview . . . . .	3
2.2 Key Concepts and Topics . . . . .	3
2.3 Learning Objectives . . . . .	3
<b>I Foundations and Theoretical Framework</b>	<b>5</b>
<b>3 Introduction to Active Matter</b>	<b>7</b>
3.1 Lecture 1 . . . . .	7
Historical context and emergence of the field . . . . .	7
Distinguishing features from equilibrium systems . . . . .	8
Classification and Examples of Active Systems . . . . .	9
3.2 Energy conversion mechanism . . . . .	9
3.3 Symmetry of motion . . . . .	10
3.4 Medium and interactions . . . . .	12
3.5 Structural arrangement . . . . .	12
3.6 Length scale and dimensionality . . . . .	13
Overview of theoretical approaches and challenges . . . . .	13
3.7 Kinetic theories . . . . .	13
3.8 Continuum field theories . . . . .	14
3.9 Agent-based and particle models . . . . .	14
Challenges in the field of active matter . . . . .	15
3.10 Experimental challenges . . . . .	15
3.11 Theoretical challenges . . . . .	16
<b>4 Statistical Mechanics Terms</b>	<b>19</b>
4.1 Brief review of equilibrium statistical mechanics . . . . .	19
Canonical ensemble and partition function . . . . .	19
Free energy and thermodynamic potentials . . . . .	21
Ergodicity and detailed balance . . . . .	23
4.2 Violation in Active Systems . . . . .	25
Brownian motion and the Langevin equation . . . . .	26
Fluctuation dissipation relation (FDT) . . . . .	26
4.3 Examples . . . . .	28
Two Brownian particles with non-uniform temperatures . . . . .	28
Chlamydomonas Swimming . . . . .	28
Primary cilia in epithelial cells . . . . .	30
<b>5 Microscopic Models of Self-propulsion</b>	<b>33</b>
5.1 Introduction: From Equilibrium Violations to Microscopic Models . . . . .	33
5.2 Run-and-Tumble Particles (RTPs) . . . . .	33

1D Run-and-Tumble with Sedimentation . . . . .	34
Mathematical Formulation in Higher Dimensions . . . . .	37
Connection to ABPs . . . . .	39
Non-equilibrium Aspects . . . . .	40
5.3 Active Brownian Particles (ABPs) . . . . .	40
Mathematical Formulation . . . . .	40
Mean Displacement . . . . .	41
Mean Square Displacement . . . . .	41
Probability Distribution . . . . .	44
Time Reversal Symmetry Breaking . . . . .	44
FDT Violation . . . . .	45
Taxonomy of Active Particle Models . . . . .	45
5.4 Swimming at Low Reynolds Number . . . . .	46
The Scallop Theorem . . . . .	46
Breaking Time-Reversibility . . . . .	47
5.5 From Swimming to Hydrodynamic Interactions . . . . .	47
The Origin of Hydrodynamic Singularities in Swimming . . . . .	49

# Chapter 1

## Active Matter Physics

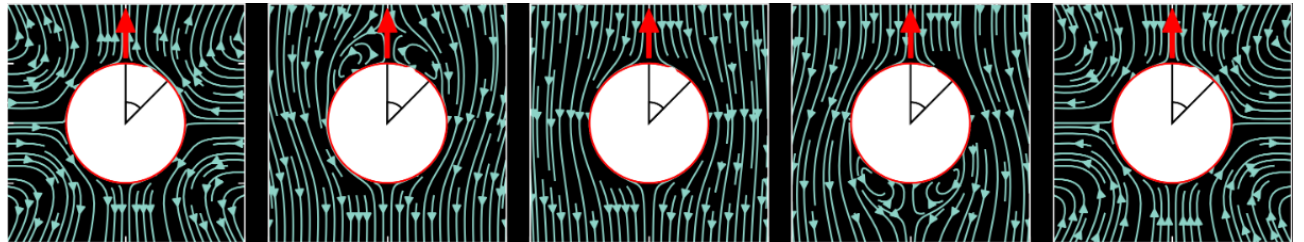


Figure 1.1: Header



## Chapter 2

# Active Matter: General Course Description

Active matter represents a rapidly evolving interdisciplinary field at the intersection of soft matter physics, biological physics, and non-equilibrium statistical mechanics. This course explores systems composed of self-propelled entities that convert energy into directed motion, giving rise to complex collective behaviors and emergent phenomena not found in traditional passive materials.

### 2.1 Course Overview

The course will examine both natural and synthetic active matter systems across multiple scales:

- **Biological active matter:** From the cytoskeleton and subcellular structures to bacterial suspensions, cell tissues, and animal groups
- **Synthetic active matter:** Including artificial microswimmers, active colloids, and engineered systems that mimic biological functionality

Students will gain a fundamental understanding of how local energy consumption at the individual unit level drives remarkable collective behaviors like self-organization, pattern formation, and spontaneous flows through non-equilibrium processes.

### 2.2 Key Concepts and Topics

- Foundations of non-equilibrium statistical physics
- Microscopic and continuum theoretical frameworks
- Experimental techniques and model systems
- Self-propulsion mechanisms and motility
- Phase transitions specific to active systems
- Emergence of collective motion and flocking
- Active turbulence and topological defects
- Mechanical properties of active materials
- Biological applications and biomimetic engineering

The course will balance theoretical principles with experimental observations, emphasizing the universal physical mechanisms that govern these diverse systems despite their different microscopic details.

### 2.3 Learning Objectives

Upon completion, students will be able to: - Identify and analyze active matter systems across disciplines - Apply theoretical models to predict behavior in active systems - Understand the key differences between equilibrium

and non-equilibrium phenomena - Connect fundamental physical principles to biological functions - Appreciate the potential applications in materials science, robotics, and biomedicine

This course is suitable for advanced undergraduate and graduate students with backgrounds in physics, engineering, biophysics, or related fields.

## **Part I**

# **Foundations and Theoretical Framework**



# Chapter 3

## Introduction to Active Matter

### 3.1 Lecture 1

#### Historical context and emergence of the field

The study of active matter emerged in the late 20th century at the intersection of soft matter physics, biophysics, and statistical mechanics. An important precursor to the field came from computer graphics, where Craig Reynolds developed the [Boids](#) simulation in 1986 - an artificial life program that demonstrated how simple rules governing individual agents could produce realistic flocking behaviors in computer animations. Earlier cellular automata models like [Conway's Game of Life](#) had also shown how simple rules could lead to complex emergent behaviors, helping establish some of the conceptual foundations for understanding collective systems.

Figure 3.1: Interactive simulation of the Boids model, where you can adjust the three key parameters that govern flocking behavior: separation (avoidance of crowding), alignment (steering towards average heading), and cohesion (steering towards center of mass).

#### The Boids Model Explained

The Boids model, developed by Craig Reynolds in 1986, simulates the flocking behavior of birds using three simple rules:

1. **Separation:** Each boid avoids crowding nearby flockmates, steering away when they get too close.
2. **Alignment:** Each boid aligns its direction of flight with nearby flockmates, matching their average velocity.
3. **Cohesion:** Each boid moves toward the center of mass of nearby flockmates, creating a tendency to stick together.

These local interaction rules, when applied to all individuals simultaneously, produce complex global behaviors that remarkably resemble natural flocking patterns. The simulation above demonstrates how adjusting these three parameters affects the emergent collective motion:

- **High separation, low alignment, low cohesion:** Dispersed individuals with minimal coordination
- **Low separation, high alignment, medium cohesion:** Coherent flocking with directional movement
- **Balanced parameters:** Natural-looking flocking behaviors with dynamic subgroup formation

This model illustrates a fundamental principle in active matter physics: complex collective behaviors can emerge from simple local rules without centralized control.

This computational model later influenced physical approaches to collective motion. Early foundational work by scientists like T. Vicsek in the 1990s established computational models for collective motion, particularly his 1995 paper introducing what is now known as the [Vicsek model](#) for self-propelled particles with alignment

interactions. Prior to this, early biological observations of collective behaviors in nature, such as bird flocking and fish schooling, had long fascinated scientists but lacked rigorous physical frameworks. The field gained significant momentum in the late 1990s with seminal papers by John Toner and Yuhai Tu, who published their groundbreaking work on flocking theory in 1995, and later Sriram Ramaswamy who developed continuum theories for active nematics.

The theoretical foundations were further strengthened by contributions from European researchers like Michael Cates (Edinburgh), Jean-François Joanny (Paris), and Jacques Prost (Paris), who developed the active gel theory to describe cytoskeletal dynamics in the mid-2000s. Simultaneously, M. Cristina Marchetti and her collaborators formulated comprehensive hydrodynamic theories for active systems across various symmetry classes. Sriram Ramaswamy made fundamental contributions through his work on active liquid crystals and the development of generic hydrodynamic theories for active matter. The pioneering work of John Toner and Yuhai Tu established the theoretical framework for understanding the emergence of long-range order in flocking systems, demonstrating how activity can stabilize orientational order even in two dimensions. Julia Yeomans (Oxford) advanced our understanding of active turbulence and topological defects in active nematics through innovative computational approaches, while Hartmut Löwen (Düsseldorf) developed influential theories for the collective behavior of active Brownian particles and motility-induced phase separation. These theoretical advances were complemented by experimental breakthroughs, notably Howard Berg's groundbreaking work in the 1970s at Harvard on bacterial chemotaxis and motility, where he developed the tracking microscope to follow individual *E. coli* bacteria and discovered their run-and-tumble motion patterns. Additional experimental contributions came from Raymond Goldstein (Cambridge) and others who established quantitative measurements of collective motion in bacterial systems.

Experimental breakthroughs with bacterial suspensions (notably work by Igor Aranson and Raymond Goldstein on *Bacillus subtilis*), cell tissues (including Xavier Trepat's research at IBEC in Barcelona on epithelial cell sheets), and synthetic active colloids (pioneered by European researchers like Jérémie Palacci (Lyon/San Diego), Julien Perrin (Paris), and Clemens Bechinger (Konstanz/Stuttgart) with light-activated Janus particles) further propelled the field forward. The development of artificial microswimmers by international collaborations involving European teams led by Roberto Di Leonardo (Rome), Ramin Golestanian (Oxford/Göttingen), and Frank Cichos (Leipzig), alongside US-based researchers like Steve Granick and Ayusman Sen, opened new avenues for creating controllable active systems outside biological contexts.

By the 2010s, active matter had developed into a distinct discipline with dedicated conferences and research groups worldwide. The establishment of specialized research centers across Europe such as the Max Planck Institute for Dynamics and Self-Organization in Göttingen, the Physics of Living Matter Group at Cambridge, the Biological Physics and Morphogenesis groups at MPIPKS Dresden, alongside the Syracuse Soft and Living Matter Program, the Center for the Physics of Biological Function at Princeton, and the Active Matter Lab at MIT reflected the field's growing importance. Major milestones included the observation of motility-induced phase separation by Michael Cates (Edinburgh) and Julien Tailleur (Paris) (2013), the discovery of topological defect motility in active nematics by Zvonimir Dogic and collaborators (2014), and the creation of the first autonomous active material capable of performing work by Daniela Wilson's group (Nijmegen) (2019). The field continues to expand with increasing interdisciplinary collaborations between physicists, biologists, materials scientists, and engineers, addressing fundamental questions in non-equilibrium physics while developing applications in biomedicine, soft robotics, and smart materials.

## Distinguishing features from equilibrium systems

Understanding how active matter systems differ from equilibrium systems is crucial for developing new theoretical frameworks and experimental approaches. The continuous energy input and self-driven nature of active matter leads to behaviors that challenge our traditional physics understanding. Consider the following key distinctions between equilibrium and active matter systems:

Feature	Equilibrium Systems	Active Matter Systems
<b>Detailed Balance</b>	Forward and reverse processes occur at equal rates	Continuously broken through energy consumption, driving the system away from equilibrium

Feature	Equilibrium Systems	Active Matter Systems
<b>Fluctuation-Dissipation Theorem</b>	Valid relationship between spontaneous fluctuations and response to external perturbations	Breaks down as fluctuations can be driven by internal activity
<b>Particle Motion</b>	Random Brownian motion	Persistent directional motion over certain timescales
<b>Statistical Distributions</b>	Follow Boltzmann statistics	Non-Boltzmann statistics, making standard thermodynamic tools inapplicable
<b>Macroscopic Currents</b>	Absent in steady states	Can sustain macroscopic currents and flux cycles even in steady states
<b>Phase Behavior</b>	Well-established equilibrium phases	Unique phase transitions with no equilibrium counterparts (e.g., motility-induced phase separation, active turbulence)
<b>Mechanical Pressure</b>	Independent of boundary properties	Can depend on properties of confining walls, violating equilibrium equations of state
<b>Energy and Entropy</b>	Minimize free energy, maximize entropy	Continuously dissipate energy and produce entropy even in steady states
<b>Time-Reversal Symmetry</b>	Dynamics appear similar when played forward or backward	Dynamics look distinctly different when played forward versus backward
<b>Force Characteristics</b>	Derivable from a potential energy function	Cannot generally be derived from a potential energy function

## Classification and Examples of Active Systems

Active matter encompasses a diverse range of systems, from biological organisms to synthetic particles, that share the common feature of continuously converting energy into systematic motion. These systems can be organized into several categories based on their energy sources, symmetries, and the nature of their interactions, providing a framework for understanding their distinct behaviors and properties.

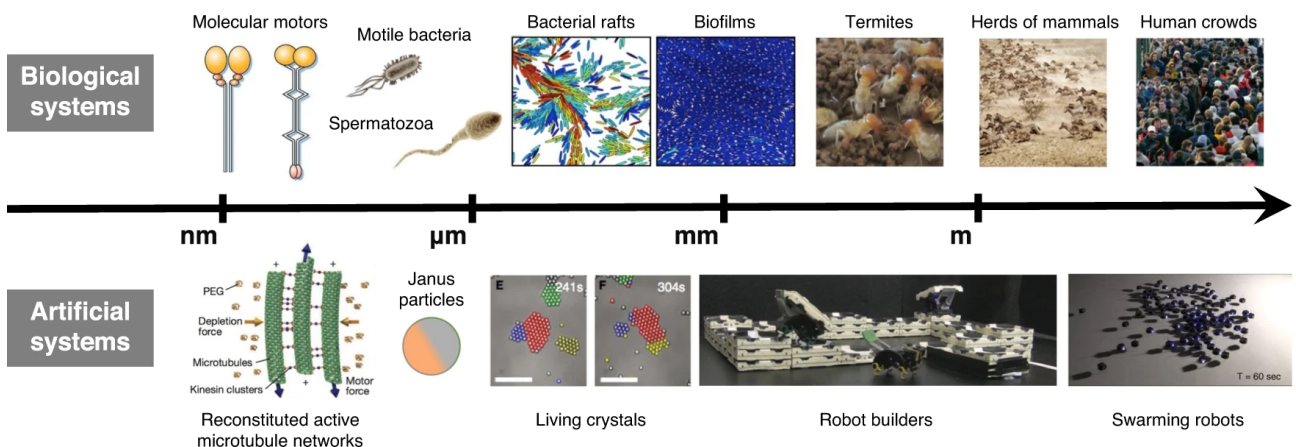


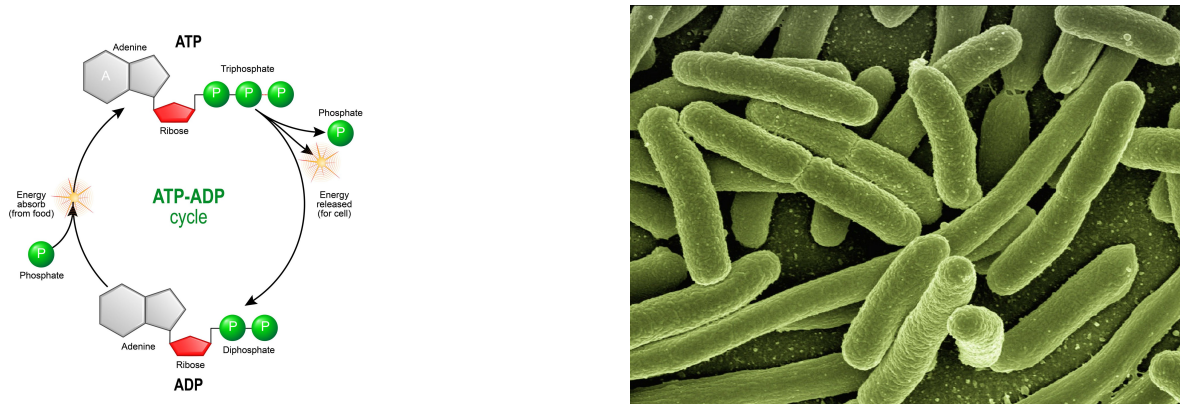
Figure 3.2: Overview of active matter systems at different scales and domains. The field spans from microscopic biological systems like cellular components to macroscopic collective behaviors and engineered synthetic systems. ([source](#))

Active matter systems can be categorized based on several key characteristics:

## 3.2 Energy conversion mechanism

- Biological active matter:** Systems that convert chemical energy (ATP, nutrients) into mechanical work (e.g., bacteria, cells, tissues). These systems span multiple scales, from molecular motors like kinesin and myosin that transport cargo along cytoskeletal filaments, to cellular components such as the

dynamic cytoskeleton that enables cell shape changes and migration. At multicellular scales, coordinated activity enables tissue morphogenesis during development, wound healing, and collective cell migration. The energy conversion typically involves ATP hydrolysis, which provides approximately  $20 \text{ kT}$  of energy per molecule, enabling these systems to perform work against thermal fluctuations. Unlike their synthetic counterparts, biological active matter often exhibits adaptive behaviors, feedback regulation, and hierarchical organization that enhances functionality and robustness.



(a) ATP hydrolysis is the primary energy source in most cellular processes (b) Bacteria like E. coli use flagella powered by molecular motors

Figure 3.3: ATP hydrolysis and bacterial motility represent key examples of chemical energy conversion in biological active matter

- **Synthetic active matter:** Engineered systems powered by external fields, chemical reactions, or light (e.g., Janus particles, active colloids). These artificial systems represent human-designed analogs to biological active matter, with scientists having precise control over their properties and behaviors. Synthetic active particles typically feature asymmetric structures or surface properties that enable self-propulsion. Common examples include Janus particles with catalyst-coated hemispheres that decompose hydrogen peroxide to create propulsion, light-activated particles that convert photonic energy into motion, and magnetically-actuated microswimmers that respond to oscillating external fields. Unlike biological systems, synthetic active matter can be designed with specific functionalities, such as targeted drug delivery, environmental remediation, or self-assembly into complex structures. Recent advances have produced programmable behaviors through responsive materials, feedback mechanisms, and even rudimentary “communication” between synthetic active agents.

### 3.3 Symmetry of motion

- **Polar active matter:** Entities with defined front-back asymmetry and directional motion (e.g., birds, fish). These systems are characterized by particles or organisms that have a clear direction of motion and can align their movement with neighbors. For example, fish schools demonstrate this through their streamlined body shape that defines a clear swimming direction, while their lateral line system helps them align with neighboring fish. Similarly, migratory birds show polar order through their aerodynamic body structure and visual alignment with flock-mates during flight. At the microscopic scale, many bacteria like E. coli exhibit polar motion through their flagellar propulsion system that creates directed swimming. The polar nature of these systems often leads to unique collective phenomena like the emergence of large-scale coherent motion and the formation of traveling bands or density waves.
- **Apolar active matter:** Systems generating motion without a defined direction (e.g., melanocytes, active nematics). These systems exhibit interesting collective behaviors despite lacking a preferred direction of motion at the individual level. For example, melanocytes, the cells responsible for skin pigmentation, extend and retract protrusions in multiple directions as they move and distribute melanin. Similarly, active nematics, such as dense suspensions of microtubules and molecular motors, generate complex flows and defect dynamics without any preferred direction of motion for individual components. The apolar

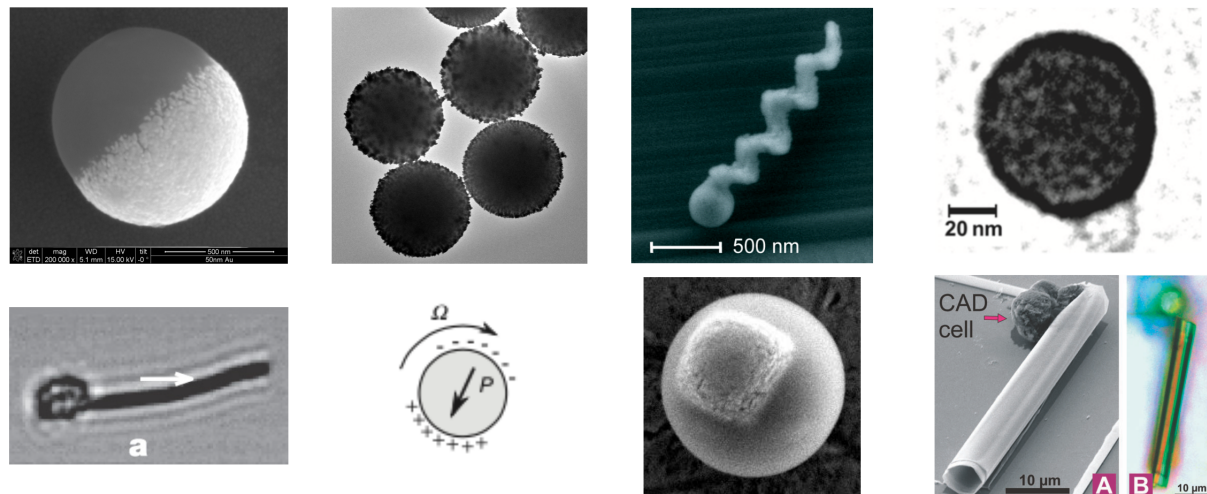


Figure 3.4: Synthetic active particles can be designed with asymmetric properties to enable self-propulsion through various mechanisms



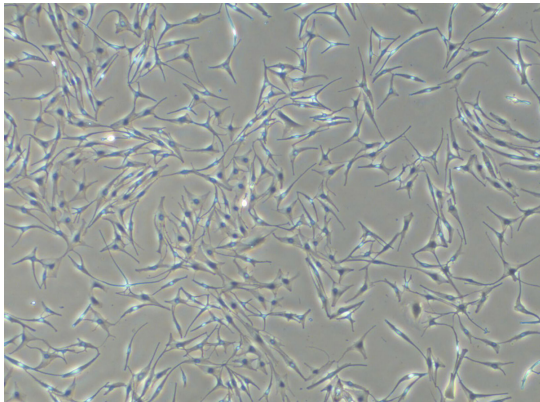
(a) Fish schools demonstrate collective motion through simple alignment rules



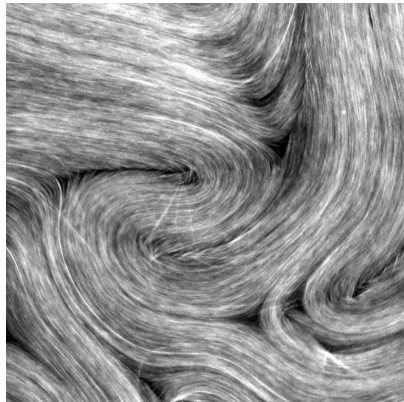
(b) Bird flocks exhibit emergent order through local interactions

Figure 3.5: Examples of polar active matter: fish schools ([source](#)) and bird flocks ([source](#))

nature of these systems often leads to unique phenomena like the spontaneous formation and annihilation of topological defects, and the emergence of active turbulence in confined geometries.



(a) Melanocyte cells showing apolar migration patterns



(b) Active nematic liquid crystals with defect patterns

Figure 3.6: Examples of apolar active matter: melanocytes ([source](#)) and active nematics ([source](#))

- **Chiral active matter:** Systems with inherent rotational motion or handedness. These systems exhibit systematic rotational motion in addition to translational movement, often due to structural asymmetry or biased force generation. Examples include bacterial flagella that rotate to create propulsion, sperm cells that swim with helical trajectories, and synthetic microswimmers with chiral shapes that spin as they move through fluid. The interplay between rotational and translational motion in these systems can lead to unique collective behaviors, such as the formation of rotating clusters or vortex arrays. At the microscopic scale, molecular motors like the bacterial flagellar motor demonstrate how nature utilizes chirality to generate motion, while at larger scales, schools of fish can form rotating vortex patterns through their collective swimming behavior.

## 3.4 Medium and interactions

- **Dry active matter:** Systems where momentum dissipates to a substrate (e.g., cells on surfaces). In these systems, the primary interaction between particles occurs through direct contact or short-range forces, as the substrate quickly dampens any long-range hydrodynamic effects. A classic example is cells crawling on a surface, where the friction with the substrate dominates the dynamics. Another example is vibrated granular layers, where energy input causes particle motion but momentum is quickly dissipated through collisions with the base plate and between particles.
- **Wet active matter:** Systems embedded in a fluid where hydrodynamic interactions dominate (e.g., bacterial suspensions). These systems exhibit complex long-range interactions mediated by the fluid, as the motion of each active particle creates flow fields that affect distant particles. Examples include swimming microorganisms in water, where the fluid flows generated by one organism can influence the motion of others several body lengths away. Active colloids in suspension also demonstrate these effects, where the chemical activity or motion of particles creates fluid flows that lead to collective behaviors and pattern formation.

## 3.5 Structural arrangement

- **Active crystals:** Ordered lattice-like arrangements with activity. These systems maintain crystalline order while individual units remain active, such as in bacterial colonies that form regular spatial patterns while each bacterium continues to move and metabolize. A key example is the formation of living crystals from light-activated colloidal particles, where the particles self-organize into a crystalline lattice while maintaining their individual motility.

- **Active glasses:** Disordered, jammed configurations with activity. Unlike traditional glasses, these systems combine structural disorder with persistent local motion, leading to unique dynamical behaviors. Examples include dense bacterial suspensions at high concentrations where cells become trapped in disordered configurations but continue to exert active forces on their neighbors, or crowded solutions of motor proteins and filaments where steric constraints create glassy dynamics despite ongoing ATP-driven activity.
- **Active fluids/gases:** Flowing systems with active components. These systems exhibit fluid-like behavior but with constituents that continuously inject energy at the microscopic scale. Examples range from dilute bacterial suspensions that show enhanced diffusion and collective motion, to dense active liquid crystals where the interplay between flow and orientational order creates complex dynamical patterns like active turbulence. In the gas-like regime, systems like midge swarms demonstrate how active particles can maintain cohesion while exhibiting fluid-like properties.

## 3.6 Length scale and dimensionality

- **Microscopic:** Cellular and subcellular systems (cytoskeleton, bacterial colonies). At this scale, active matter emerges from molecular motors like kinesin and dynein walking along cytoskeletal filaments, or the collective motion of bacterial cells in colonies. The cytoskeleton itself is a fascinating example where networks of actin filaments and microtubules, driven by ATP-powered molecular motors, create complex dynamics essential for cell function and division.
- **Mesoscopic:** Tissue and organ-level organizations. At the tissue level, collective cell behavior leads to emergent phenomena like wound healing and morphogenesis during development. Epithelial tissues demonstrate active matter dynamics through coordinated cell migration and mechanical force transmission between neighboring cells. These intermediate scales bridge individual cell behavior with organ-level function.

[https://youtu.be/QF1BW9fFhig?si=nSWW1lDf8Xw\\_RpS5](https://youtu.be/QF1BW9fFhig?si=nSWW1lDf8Xw_RpS5)

Figure 3.7: Time-lapse microscopy of Drosophila embryo development showing gastrulation and tissue folding - a striking example of how active matter principles govern morphogenesis. The coordinated cell shape changes and movements create complex three-dimensional structures from an initially simple tissue sheet. [source](#)

- **Macroscopic:** Animal groups, human crowds. Large-scale collective behaviors emerge in systems like bird flocks, fish schools, and human crowds in urban environments. These systems demonstrate how simple interaction rules between individuals can create complex, coordinated motion patterns that span hundreds or thousands of times the size of individual agents. Traffic flow and pedestrian dynamics are particularly relevant examples for urban planning and crowd safety.
- **Quasi-2D vs. 3D systems:** Systems confined to surfaces vs. fully three-dimensional systems. Many active matter systems are effectively two-dimensional, like bacterial colonies growing on agar plates or cells migrating on substrates. These confined geometries often simplify both experimental observation and theoretical analysis. In contrast, true three-dimensional systems like bacterial suspensions in fluid or cell movement in tissue matrices exhibit additional complexities due to hydrodynamic interactions and the full range of possible motion directions.

## Overview of theoretical approaches and challenges

The theoretical description of active matter draws from and extends multiple branches of physics:

## 3.7 Kinetic theories

- **Boltzmann-like approaches:** Describing probability distributions of particle positions and orientations in active systems. For example, in bacterial suspensions, this approach tracks how the probability of finding bacteria with specific positions and swimming directions evolves over time. The key difference from classical Boltzmann equations is the inclusion of self-propulsion forces and alignment interactions.

These equations have been particularly successful in describing the transition from disordered to ordered states in active systems like bird flocks and fish schools.

- **Fokker-Planck equations:** Capturing the evolution of probability densities in phase space by incorporating both deterministic and stochastic effects. In active matter, these equations describe how probability distributions change due to systematic forces (like self-propulsion), random fluctuations (thermal or active noise), and interactions between particles. For instance, they can model how Janus particles move under the influence of chemical gradients while experiencing rotational diffusion, or how swimming bacteria respond to chemical attractants while subject to tumbling events.
- **Smoluchowski equations:** Modeling overdamped dynamics common in biological active systems where inertial effects are negligible compared to viscous forces. These equations are particularly relevant for microscopic swimmers like bacteria or colloidal particles where the Reynolds number is very small. They have been successfully applied to describe phenomena like bacterial chemotaxis, the collective motion of cell populations, and the dynamics of motor proteins along cytoskeletal filaments. A classic example is modeling E. coli's run-and-tumble motion, where the Smoluchowski equation – the overdamped limit of the Fokker-Planck equation – captures the interplay between directed swimming and random reorientations.

## 3.8 Continuum field theories

- **Toner-Tu theory:** A hydrodynamic framework that describes collective motion in flocking systems by incorporating broken continuous symmetry. This theory is particularly powerful for analyzing large systems, where it predicts true long-range order can exist even in two dimensions, in contrast to equilibrium systems. While real flocks are finite, the theory provides insights into large-scale behaviors like the scale-free correlations observed in starling murmurations, where thousands of birds maintain coherent motion despite environmental perturbations.
- **Active gel theories:** These theories extend traditional liquid crystal physics by incorporating force-generating active stresses. They are particularly successful in describing biological materials like the cell cytoskeleton, where molecular motors generate internal forces. A key example is explaining the spontaneous flows observed in actomyosin networks, where myosin motors walking along actin filaments create large-scale coherent motion.
- **Active nematics:** Field theories that describe systems with orientational order but no polar direction, driven out of equilibrium by active stresses. These theories have been instrumental in understanding phenomena like the chaotic dynamics of microtubule-kinesin mixtures, where energy input from molecular motors leads to the continuous creation, motion, and annihilation of topological defects, resulting in active turbulence.
- **Phase field models:** Mathematical frameworks that track the evolution of interfaces and boundaries in active systems without explicitly tracking individual particles. These models have been successfully applied to describe phenomena like cell membrane deformation during motility, tissue morphogenesis, and the dynamics of active droplets. For instance, they can capture how a crawling cell changes shape and moves by coupling chemical signals to mechanical deformations of the cell membrane.

## 3.9 Agent-based and particle models

- **Vicsek model:** The foundational model for collective motion where particles move at constant speed and align their direction with neighbors within a certain radius, subject to noise. For example, in simulating bird flocks, each bird adjusts its direction to match the average flight direction of nearby birds, plus some random variation. This simple rule produces rich collective behaviors like the transition from disordered motion at high noise to coordinated flocking at low noise.
- **Active Brownian particles:** Self-propelled particles that maintain constant speed but undergo rotational diffusion, leading to persistent random walks. A classic example is light-activated Janus colloids – microscopic particles with one hemisphere coated in a light-responsive material. Under illumination, these particles swim in a directed manner but gradually change direction due to thermal fluctuations, resulting in motion that is ballistic at short times but diffusive at long times.

- **Run-and-tumble models:** These models capture the motion pattern of bacteria like E. coli, which alternate between straight “runs” and random “tumbles.” During runs, the bacteria swim in nearly straight lines using their flagella. Tumbles occur when the flagella bundle comes apart, causing the cell to randomly reorient. This mechanism allows bacteria to effectively explore their environment and respond to chemical gradients through biased random walks.
- **Active Ornstein-Uhlenbeck particles:** A model incorporating temporal correlations in the active propulsion force, leading to more realistic descriptions of biological swimmers. For instance, in modeling the motion of algae like Chlamydomonas, the swimming force isn’t purely random but shows correlations over the time scale of the flagellar beat cycle. This correlation produces more accurate predictions of diffusion and clustering behaviors compared to simpler active particle models.

### Challenges in the field of active matter

The scientific study of active matter presents several key theoretical and experimental challenges that continue to motivate research and technological innovation in the field:

## 3.10 Experimental challenges

- **Diversity in propulsion mechanisms and functionality:** Creating synthetic active particles with diverse propulsion strategies and functional capabilities remains challenging. Current systems are largely limited to chemical catalysis, light activation, or magnetic actuation. Beyond propulsion, developing particles capable of force generation, information processing, and programmable behaviors through compartmentalization and feedback control is crucial. This includes systems that can adapt their behavior based on environmental cues or machine learning algorithms.
- **Multi-component systems:** Developing heterogeneous active matter systems with different types of particles that can interact and coordinate. For example, combining light-activated and chemically-powered particles, or integrating passive and active components to create hierarchical structures with emergent behaviors.
- **Measurement techniques:** Developing methods to track fast dynamics across multiple scales. Active matter systems often exhibit complex spatiotemporal dynamics that require simultaneous tracking of individual particles and collective behaviors. High-speed imaging, particle tracking, and flow visualization techniques must be adapted to capture both the rapid motion of individual active units and the slower evolution of large-scale patterns.
- **System preparation:** Creating synthetic particles with programmable behaviors and functions. The synthesis of active colloids requires careful control over particle size, shape, surface chemistry, and catalyst distribution, as well as the integration of responsive elements that enable specific functionalities. For instance, incorporating multiple catalytic or stimuli-responsive domains to create particles capable of complex tasks remains technically challenging.
- **Boundary conditions:** Controlling and characterizing interactions with surfaces. Active matter systems are highly sensitive to boundary conditions, which can significantly influence their behavior. Creating well-defined boundaries while maintaining activity and avoiding unwanted surface effects requires careful experimental design and characterization.
- **Energy input:** Maintaining steady, uniform activation across synthetic systems. Whether through chemical fuel concentration, light intensity, magnetic fields, or electric fields, ensuring uniform activation throughout the sample volume is crucial. Challenges include maintaining constant H<sub>2</sub>O<sub>2</sub> concentration for catalytic swimmers or uniform illumination for light-activated particles.
- **Time limitations:** Managing fuel depletion and particle degradation while maintaining function. Synthetic active systems face challenges like catalyst poisoning, fuel consumption, and photobleaching that can impair their ability to perform desired tasks. For chemical swimmers, local fuel depletion can create concentration gradients that affect particle behavior, while light-activated systems may suffer from photodamage over time.

- **Imaging limitations:** Balancing spatial and temporal resolution with field of view. Active matter often requires both high-resolution imaging to track individual particles and wide-field observation to capture collective effects. This creates technical challenges in microscopy and imaging systems, particularly for three-dimensional systems.
- **Parameter space:** Exploring vast parameter spaces with limited resources. Synthetic active matter systems have many tunable parameters including particle size, shape, surface chemistry, fuel concentration, and external field strengths. Systematically exploring these parameters while maintaining experimental consistency requires significant time and resources.
- **System integration:** Incorporating active matter into functional devices or materials while maintaining desired behaviors. Synthetic active matter experiments require careful integration with other components while preserving activity and function. Creating stable, reliable systems that can operate under real-world conditions presents significant engineering challenges.

### 3.11 Theoretical challenges

- **Bridging scales:** Connecting microscopic mechanisms to macroscopic behaviors. Active matter systems often exhibit behaviors across many orders of magnitude in length and time scales, making it challenging to track how molecular-level processes give rise to large-scale collective phenomena. For example, in bacterial colonies, individual cell motility and interactions must be connected to population-level dynamics and pattern formation, requiring sophisticated multi-scale modeling approaches.
- **Non-equilibrium statistical mechanics:** Developing systematic frameworks beyond equilibrium concepts. Traditional statistical mechanics relies heavily on concepts like detailed balance and the fluctuation-dissipation theorem, which break down in active systems due to continuous energy input. The lack of an energy minimum principle or equivalent organizing framework makes it difficult to develop general theories for non-equilibrium steady states.
- **Topological effects:** Understanding defect nucleation, motion, and interactions. In active systems, topological defects can spontaneously nucleate, move, and interact in ways fundamentally different from their equilibrium counterparts due to the continuous energy input. The coupling between defect dynamics and active stresses creates complex feedback loops that are challenging to describe theoretically.
- **Capturing boundary effects:** Modeling how boundaries and confinement influence active dynamics. Active matter systems exhibit unique responses to boundaries that can qualitatively change their behavior, such as accumulation at walls or spontaneous circulation in confined geometries. These boundary effects often depend non-trivially on microscopic details of both the active particles and the confining surfaces.
- **Incorporating disorder and heterogeneity:** Addressing realistic imperfections in theoretical frameworks. Real active matter systems invariably contain disorder and heterogeneity in particle properties, interactions, and environmental conditions. Incorporating these imperfections while maintaining theoretical tractability requires careful balance between complexity and analytical feasibility.
- **Coupling to external fields:** Describing responses to gradients, flows, and applied fields. Active matter systems show complex and often counterintuitive responses to external fields, such as negative mobility or upstream swimming in flows. The interplay between internal activity and external forcing creates rich dynamics that challenge our theoretical understanding.
- **Information flow:** Quantifying information processing in active biological systems. Biological active matter systems process and respond to information in sophisticated ways, from bacterial chemotaxis to collective decision making in animal groups. Developing theoretical frameworks to quantify and model this information processing remains a major challenge.
- **Perception-reaction delays:** Biological active matter processes information at rates significantly slower than modern computers due to the inherent limitations of biochemical signaling pathways. These delays between perception and response manifest in various active systems, from human driving behavior in daily traffic to collective animal movement patterns. Such temporal gaps between stimulus detection and behavioral adjustment critically influence numerous dynamical states in active matter. To compensate for this inherent slowness, biological systems have evolved predictive mechanisms that anticipate future

states and allow for more effective responses despite processing limitations. Dealing with such delays is a considerable challenge for theoretical modelling.

- **Predictive power:** Developing theories with quantitative predictive capabilities for experiments. The complexity and non-equilibrium nature of active matter systems often leads to theories that are qualitative rather than quantitative in nature. Making precise, testable predictions requires better understanding of the relevant control parameters and their relationships to observable phenomena.



# Chapter 4

## Statistical Mechanics Terms

### 4.1 Brief review of equilibrium statistical mechanics

Equilibrium statistical mechanics may seem like a contradictory starting point for understanding fundamentally non-equilibrium phenomena in active matter. However, we begin with these concepts precisely because understanding how and why active systems violate equilibrium principles illuminates their unique properties. In this section, we review key equilibrium concepts that provide a crucial reference frame against which we can measure and characterize the non-equilibrium nature of active systems.

#### Canonical ensemble and partition function

For a system in thermal equilibrium with a heat bath at temperature  $T$  not exchanging particles with the environment, the probability of finding the system in a microstate with phase space coordinates  $\Gamma = \{\mathbf{q}, \mathbf{p}\}$  is given by the Boltzmann distribution:

$$P(\Gamma) = \frac{1}{Z} e^{-\beta H(\Gamma)}$$

where  $\beta = 1/(k_B T)$ ,  $k_B$  is Boltzmann's constant,  $H(\Gamma)$  is the Hamiltonian of the system, and  $Z$  is the partition function:

$$Z = \frac{1}{h^{3N} N!} \int e^{-\beta H(\Gamma)} d\Gamma$$

In this expression,  $h$  is Planck's constant,  $N$  is the number of particles, and the factors  $h^{3N}$  and  $N!$  account for the quantum uncertainty principle and the indistinguishability of identical particles, respectively. This normalization ensures that the partition function is dimensionless.

In physical terms, the Boltzmann distribution reflects how energy is partitioned among the available states at thermal equilibrium. States with lower energy are exponentially more likely to be occupied than states with higher energy. For active matter systems, this distribution is significantly altered because energy is continuously injected at the microscopic level, driving the system away from this equilibrium distribution. Indeed, active systems generally cannot be described by a time-independent Hamiltonian at all, as they involve non-conservative forces.

The partition function is central to statistical mechanics as it connects microscopic properties to macroscopic observables. For instance, the average energy is:

$$\langle H \rangle = -\frac{\partial \ln Z}{\partial \beta}$$

This relationship highlights how the partition function serves as a generating function for thermodynamic quantities. When studying active matter, we'll see that traditional partition functions often cannot be defined because these systems don't explore phase space according to Boltzmann statistics.

### Sedimentation Example

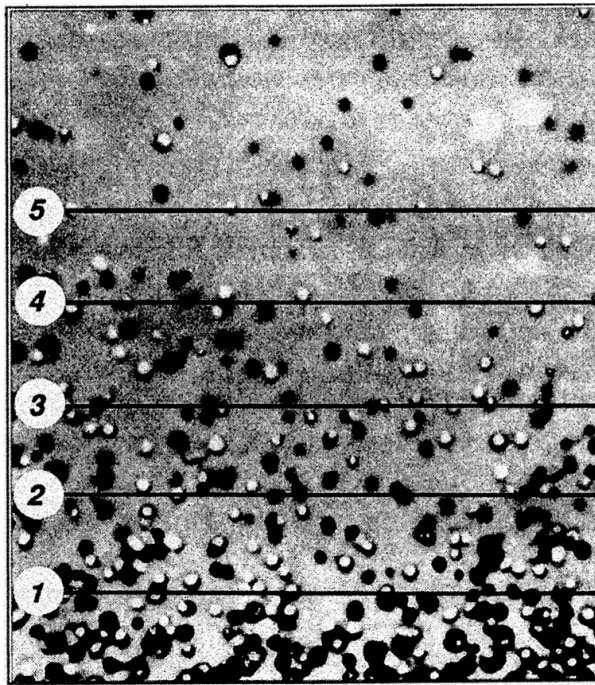


Figure 4.1: Perrin's sedimentation experiments. The exponential decay in the number density of colloidal particles with height directly confirmed the Boltzmann distribution and provided key evidence for the atomic theory of matter.

A clear demonstration of the Boltzmann distribution's power can be derived from the canonical partition function using the barometric distribution of particles in a gravitational field. Consider colloidal particles suspended in a fluid in a gravitational field  $g$ .

The Hamiltonian for a particle at height  $h$  with momentum  $p$  is:

$$H(h, p) = \frac{p^2}{2m} + mgh$$

where the first term represents the kinetic energy and the second term is the gravitational potential energy. For this system, we can construct the partition function by integrating over all possible heights and momenta:

$$Z = \int_0^\infty \int_{-\infty}^\infty e^{-\beta H(h,p)} dp dh = \int_0^\infty \int_{-\infty}^\infty e^{-\beta(\frac{p^2}{2m} + mgh)} dp dh$$

This can be separated into:

$$Z = \int_{-\infty}^\infty e^{-\beta \frac{p^2}{2m}} dp \cdot \int_0^\infty e^{-\beta mgh} dh$$

The momentum integral gives  $\sqrt{\frac{2\pi m}{\beta}}$ , while the height integral yields  $\frac{1}{\beta mg}$ , resulting in:

$$Z = \sqrt{\frac{2\pi m}{\beta}} \cdot \frac{1}{\beta mg} = \sqrt{\frac{2\pi m}{\beta^3 m^2 g^2}}$$

The probability density for finding a particle at height  $h$  (integrating over all momenta) is:

$$P(h) = \frac{\int_{-\infty}^{\infty} e^{-\beta(\frac{p^2}{2m} + mgh)} dp}{Z} = \frac{\sqrt{\frac{2\pi m}{\beta}} \cdot e^{-\beta mgh}}{\sqrt{\frac{2\pi m}{\beta}} \cdot \frac{1}{\beta mg}}$$

From this, we can derive the number density  $n(h)$  by multiplying by the total number of particles  $N$ :

$$n(h) = N \cdot P(h) = N \beta m g e^{-\beta mgh}$$

If we define  $n_0$  as the density at  $h = 0$ , then  $n_0 = N \beta m g$ , and we obtain:

$$n(h) = n_0 e^{-\beta mgh} = n_0 e^{-\frac{mgh}{k_B T}}$$

Taking the logarithm of both sides:

$$\ln\left(\frac{n(h)}{n_0}\right) = -\beta mgh = -\frac{mgh}{k_B T}$$

This direct connection between the Hamiltonian, partition function, and the observable barometric distribution provides a compelling experimental verification of statistical mechanics. Jean Perrin used this relationship in 1908 to experimentally determine Avogadro's number and provide crucial evidence for the atomic theory of matter. Today, similar experiments with colloidal particles serve as textbook demonstrations of statistical mechanics in action.

## Free energy and thermodynamic potentials

The Helmholtz free energy is a thermodynamic potential that determines the maximum useful work obtainable from a closed system at constant temperature and volume. Named after German physicist Hermann von Helmholtz, it represents the amount of energy available to do non-expansion work. The Helmholtz free energy is particularly relevant in statistical mechanics because it serves as the fundamental bridge between microscopic properties (encoded in the partition function) and macroscopic thermodynamic behavior. For systems in the canonical ensemble—where the number of particles, volume, and temperature are fixed—the Helmholtz free energy provides the appropriate thermodynamic potential whose minimum determines the equilibrium state.

The Helmholtz free energy  $F$  is related to the partition function by:

$$F = -k_B T \ln Z = -k_B T \ln \left( \frac{1}{h^{3N} N!} \int e^{-\beta H(\Gamma)} d\Gamma \right)$$

where the normalization factor  $\frac{1}{h^{3N} N!}$  ensures proper dimensionless units in the partition function, with  $h$  being Planck's constant and  $N$  the number of particles.

We can rewrite this as  $F = E - TS$ , explicitly showing the competition between the enthalpic (energy) and entropic contributions:

$$F = \langle H \rangle - TS$$

where  $\langle H \rangle$  is the average energy:

$$\langle H \rangle = -\frac{\partial \ln Z}{\partial \beta} = \frac{\int H(\Gamma) e^{-\beta H(\Gamma)} d\Gamma}{\int e^{-\beta H(\Gamma)} d\Gamma}$$

and  $S$  is the entropy:

$$S = -\left(\frac{\partial F}{\partial T}\right)_V = k_B \ln Z + \frac{\langle H \rangle}{T}$$

At equilibrium, minimizing the free energy involves a fundamental competition between:

1. **Energy minimization:** The system tends to occupy low-energy states to minimize  $\langle H \rangle$
2. **Entropy maximization:** The system tends to spread over many accessible states to maximize  $S$

The Boltzmann distribution  $P(\Gamma) = \frac{1}{Z}e^{-\beta H(\Gamma)}$  represents the optimal compromise between these competing tendencies. For systems with fixed particle number, volume, and temperature (canonical ensemble), this distribution precisely minimizes the free energy subject to the constraints of the canonical ensemble.

The principle of free energy minimization is particularly important for understanding the contrast with active systems. In active matter, free energy is constantly being pumped into the system through microscopic driving mechanisms (e.g., molecular motors in cell cytoskeleton, metabolic processes in bacteria, or artificial propulsion mechanisms in synthetic swimmers). These systems involve non-conservative forces that cannot be derived from a Hamiltonian, so they cannot be described by a minimum free energy principle, which is a fundamental departure from equilibrium thermodynamics.

### Harmonic Oscillator Example

The harmonic oscillator provides another illuminating example of equilibrium statistical mechanics. Consider a Brownian particle in a harmonic potential  $U(x) = \frac{1}{2}kx^2$  provided by some highly focused light beam. Here  $k$  is the spring constant.

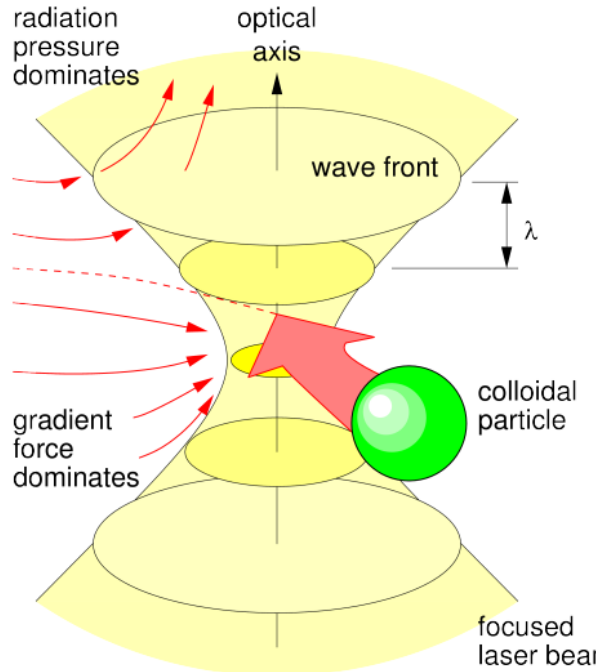


Figure 4.2: Sketch of a colloidal particle trapped in the focus of a microscopy lens due to electromagnetic forces. [source](#)

The particle experiences both a restoring force and random thermal kicks from the surrounding fluid. The Hamiltonian for this system is:

$$H(x, p) = \frac{p^2}{2m} + \frac{1}{2}kx^2$$

where  $m$  is the particle mass,  $x$  is position, and  $p$  is momentum. The partition function is:

$$Z = \int_{-\infty}^{\infty} \int_{-\infty}^{\infty} e^{-\beta H(x,p)} dx dp = \int_{-\infty}^{\infty} e^{-\beta \frac{p^2}{2m}} dp \int_{-\infty}^{\infty} e^{-\beta \frac{1}{2}kx^2} dx$$

Evaluating these Gaussian integrals:

$$Z = \sqrt{\frac{2\pi m}{\beta}} \sqrt{\frac{2\pi}{\beta k}} = \frac{2\pi}{\beta\omega_0}$$

where  $\omega_0 = \sqrt{k/m}$  is the natural frequency of the oscillator.

The probability density for finding the particle at position  $x$  is:

$$P(x) = \sqrt{\frac{\beta k}{2\pi}} e^{-\beta \frac{1}{2} kx^2}$$

This Gaussian distribution has variance  $\sigma^2 = \frac{1}{\beta k} = \frac{k_B T}{k}$ .

The equipartition theorem states that each quadratic term in the Hamiltonian contributes  $\frac{1}{2}k_B T$  to the average energy:

$$\left\langle \frac{p^2}{2m} \right\rangle = \left\langle \frac{1}{2}kx^2 \right\rangle = \frac{1}{2}k_B T$$

Therefore, the mean-square displacement of the particle is:

$$\langle x^2 \rangle = \frac{k_B T}{k}$$

This simple relation demonstrates how thermal energy causes the particle to explore the potential well, with the stiffness of the spring determining the confinement. Stiffer springs (larger  $k$ ) lead to smaller position fluctuations.

## Ergodicity and detailed balance

A key assumption in equilibrium statistical mechanics is ergodicity—the equivalence between time averages and ensemble averages:

$$\langle A \rangle_{\text{time}} = \lim_{T \rightarrow \infty} \frac{1}{T} \int_0^T A(t) dt = \langle A \rangle_{\text{ensemble}}$$

In practical terms, ergodicity means that if you observe a single system for a sufficiently long time, it will eventually visit all microscopic states consistent with its macroscopic constraints, allowing time averages to equal ensemble averages. Active matter systems often violate ergodicity by persistently exploring only a subset of the available phase space due to their self-propulsion mechanisms. This has profound implications for both experimental measurements and theoretical descriptions of active systems.

Equilibrium dynamics satisfies detailed balance, a microscopic time-reversal symmetry condition. For transitions between states  $i$  and  $j$  with rates  $W_{i \rightarrow j}$  and  $W_{j \rightarrow i}$ :

$$\frac{W_{i \rightarrow j}}{W_{j \rightarrow i}} = \frac{P_j^{\text{eq}}}{P_i^{\text{eq}}} = e^{-\beta(E_j - E_i)}$$

Detailed balance ensures that there are no net probability currents in equilibrium.

## Application to Sedimentation

In the sedimentation example, we can apply detailed balance to particles moving between different heights in a gravitational field. Consider transitions between heights  $h_i$  and  $h_j$ :

- The equilibrium probability to find a particle at height  $h$  is  $P(h) \propto e^{-\beta mgh}$
- For a particle moving from height  $h_i$  to a higher position  $h_j$ , the energy difference is  $\Delta E = mg(h_j - h_i)$

By detailed balance, the transition rates must satisfy:

$$\frac{W_{h_i \rightarrow h_j}}{W_{h_j \rightarrow h_i}} = \frac{e^{-\beta mgh_j}}{e^{-\beta mgh_i}} = e^{-\beta mg(h_j - h_i)}$$

This reveals that upward transitions (against gravity) are exponentially suppressed compared to downward transitions. If we observe the system over time, we would see particles moving both up and down, but with precisely balanced rates that maintain the exponential density profile.

This balance has profound implications for trajectory reversibility. In equilibrium systems, detailed balance ensures that for any specific trajectory  $\gamma$  a particle takes from height  $h_i$  to  $h_j$  over a time interval  $[0, t]$ , the time-reversed trajectory  $\bar{\gamma}$  (the same path followed backward in time) from  $h_j$  to  $h_i$  occurs with a probability that differs only by the Boltzmann factor:

$$\frac{P[\gamma]}{P[\bar{\gamma}]} = e^{-\beta mg(h_j - h_i)}$$

This microscopic reversibility means that if we filmed the motion of an equilibrium system and played the recording backward, the reversed motion would be statistically indistinguishable from the forward motion (when properly weighted by the equilibrium probabilities). For particles in sedimentation, this time-reversal symmetry ensures that no systematic currents exist in the steady state—particles may diffuse up and down, but any apparent “uphill” motion is precisely balanced by “downhill” motion, maintaining the exponential density profile without net circulation in phase space.

### Connecting to Fluctuation Theorems

The relationship between detailed balance, trajectory reversibility, and sedimentation connects directly to fluctuation theorems, which provide a broader framework for understanding non-equilibrium systems:

#### Connection to Fluctuation Theorems

The trajectory reversibility we described for equilibrium systems (where  $\frac{P[\gamma]}{P[\bar{\gamma}]} = e^{-\beta mg(h_j - h_i)}$ ) is actually a special case of more general fluctuation theorems that apply even to non-equilibrium systems. These theorems quantify the probability of observing trajectories that appear to violate the second law of thermodynamics.

For the sedimentation example, the key connections are:

1. **Crooks Fluctuation Theorem:** This relates the probability of forward and reverse trajectories to the entropy production:

$$\frac{P[\gamma]}{P[\bar{\gamma}]} = e^{\beta(W - \Delta F)} = e^{\Delta S_{tot}/k_B}$$

Where  $W$  is the work done,  $\Delta F$  is the free energy difference, and  $\Delta S_{tot}$  is the total entropy production.

2. **Equilibrium Special Case:** When detailed balance is satisfied (as in passive sedimentation),  $W = \Delta F = mg(h_j - h_i)$  and  $\Delta S_{tot} = 0$ , recovering our earlier result.
3. **Active Systems:** For active particles in sedimentation, we have additional work from active forces, leading to:

$$\frac{P[\gamma]}{P[\bar{\gamma}]} = e^{\beta mg(h_j - h_i) + \Delta S_{act}/k_B}$$

Where  $\Delta S_{act} > 0$  is the entropy production due to activity.

### **i** Master Equation Formulation

Detailed balance can be elegantly formulated in terms of a master equation, which provides a powerful framework for understanding the time evolution of probability distributions. The master equation describes how the probability  $P_i(t)$  of finding the system in state  $i$  evolves over time:

$$\frac{dP_i(t)}{dt} = \sum_j [W_{j \rightarrow i} P_j(t) - W_{i \rightarrow j} P_i(t)]$$

where  $W_{j \rightarrow i}$  is the transition rate from state  $j$  to state  $i$ .

The first term represents probability flowing into state  $i$  from all other states  $j$ , while the second term represents probability flowing out of state  $i$  to all other states  $j$ .

#### Detailed Balance as a Stronger Condition

At steady state, the left-hand side of the master equation equals zero, meaning:

$$\sum_j [W_{j \rightarrow i} P_j - W_{i \rightarrow j} P_i] = 0$$

However, detailed balance imposes a much stronger condition - that each term in this sum must individually equal zero:

$$W_{j \rightarrow i} P_j^{eq} = W_{i \rightarrow j} P_i^{eq} \quad \text{for all pairs } i, j$$

This is equivalent to requiring that the net probability current between any two states vanishes at equilibrium.

#### Application to Sedimentation

For sedimentation, we can discretize the height into levels  $h_i$ . The master equation becomes:

$$\frac{dP(h_i, t)}{dt} = \sum_j [W_{h_j \rightarrow h_i} P(h_j, t) - W_{h_i \rightarrow h_j} P(h_i, t)]$$

Detailed balance requires:

$$W_{h_j \rightarrow h_i} P^{eq}(h_j) = W_{h_i \rightarrow h_j} P^{eq}(h_i)$$

Substituting the Boltzmann distribution  $P^{eq}(h) \propto e^{-\beta mgh}$ :

$$W_{h_j \rightarrow h_i} e^{-\beta mgh_j} = W_{h_i \rightarrow h_j} e^{-\beta mgh_i}$$

Rearranging:

$$\frac{W_{h_i \rightarrow h_j}}{W_{h_j \rightarrow h_i}} = \frac{e^{-\beta mgh_j}}{e^{-\beta mgh_i}} = e^{-\beta mg(h_j - h_i)}$$

This recovers our previous expression for detailed balance in sedimentation.

## 4.2 Violation in Active Systems

For active particles, we would have additional terms in the master equation representing the active motion. The condition above would no longer be satisfied, and instead, we would find:

$$W_{h_j \rightarrow h_i}^{act} P^{ss}(h_j) \neq W_{h_i \rightarrow h_j}^{act} P^{ss}(h_i)$$

where  $P^s$ s denotes the non-equilibrium steady state distribution.

## Brownian motion and the Langevin equation

Brownian motion provides a simple yet powerful model for understanding thermal fluctuations. The Langevin equation describes the motion of a Brownian particle:

$$m \frac{d^2x}{dt^2} = -\gamma \frac{dx}{dt} - \frac{dU(x)}{dx} + \xi(t)$$

where  $\gamma$  is the friction coefficient,  $U(x)$  is the potential energy, and  $\xi(t)$  is Gaussian white noise with:

$$\langle \xi(t) \rangle = 0, \quad \langle \xi(t)\xi(t') \rangle = 2\gamma k_B T \delta(t - t')$$

The noise amplitude is related to the friction coefficient through the fluctuation-dissipation relation, a consequence of thermal equilibrium. This relation embodies a deep physical principle: the same microscopic processes that cause energy dissipation (friction) also generate fluctuations (noise), with temperature determining their relative strength.

Understanding the Langevin equation is crucial as it serves as a conceptual bridge between equilibrium and non-equilibrium physics. When modeling active particles, we extend this framework by adding a self-propulsion term. The simplest model of an active Brownian particle (ABP) incorporates a propulsion force of constant magnitude but with a direction that changes through rotational diffusion:

$$\gamma \frac{d\mathbf{r}}{dt} = -\nabla U(\mathbf{r}) + \gamma v_0 \mathbf{n}(t) + \xi(t)$$

where  $v_0$  represents the swimming speed and  $\mathbf{n}(t)$  is a unit vector undergoing rotational diffusion. This seemingly simple modification profoundly transforms the physics, leading to enhanced diffusion, boundary accumulation, and novel collective behaviors unlike anything seen in passive systems.

In many situations relevant to colloidal systems and active matter, inertial effects can be neglected, leading to the overdamped limit of the Langevin equation:

$$\gamma \frac{dx}{dt} = -\frac{dU(x)}{dx} + \xi(t)$$

This overdamped approximation accurately describes microscopic active systems such as bacterial suspensions, catalytic Janus particles, and colloidal rollers. In these systems, the Reynolds number is extremely low (typically  $10^{-5}$  to  $10^{-2}$ ), meaning viscous forces dominate over inertial forces. Consequently, particles stop moving almost instantaneously when propulsion ceases—a counterintuitive behavior compared to our macroscopic experience where objects continue moving due to inertia.

The Langevin framework will serve as our starting point for understanding how active systems systematically violate equilibrium principles. As we explore further, we'll see that active matter requires expanding our theoretical tools beyond equilibrium statistical mechanics to account for the continuous energy input that drives these fascinating systems far from equilibrium.

## Fluctuation dissipation relation (FDT)

The Fluctuation-Dissipation Theorem (FDT) is a cornerstone principle in equilibrium statistical mechanics that connects two seemingly different phenomena:

1. The random thermal fluctuations that naturally occur in a system at equilibrium
2. How that same system responds when deliberately disturbed by an external force

Mathematically, the FDT is often most elegantly expressed in frequency space:

$$\chi''(\omega) = \frac{\omega}{2k_B T} S(\omega)$$

where  $\chi''(\omega)$  is the imaginary part of the frequency-dependent susceptibility (describing the dissipative response to perturbations), and  $S(\omega)$  is the power spectral density of the equilibrium fluctuations.

Alternatively, using the full complex susceptibility:

$$\chi(\omega) = \frac{1}{k_B T} \int_0^\infty C(t) e^{i\omega t} dt$$

The FDT tells us that for systems in thermal equilibrium, these two behaviors are directly linked through temperature. This means we can learn how a system will respond to an external force simply by observing how it naturally fluctuates when left alone—a profound connection that becomes particularly transparent in the frequency domain.

### Trapped Brownian particle

Consider a microscopic particle trapped in an optical tweezer (essentially a harmonic potential created by focused laser light). The particle jiggles around randomly due to collisions with surrounding fluid molecules - these are its natural thermal fluctuations.

The FDT tells us that by simply measuring how much this particle naturally jiggles (its position fluctuations), we can predict exactly how far it would move if we applied a small external force to it.

Let's examine this for a colloidal particle in a one-dimensional harmonic trap, described by the overdamped Langevin equation:

$$\gamma \frac{dx}{dt} = -kx + \xi(t) + F_{ext}(t)$$

where:

- $\gamma$  is the friction coefficient (resistance to motion)
- $k$  is the trap stiffness (strength of the restoring force)
- $\xi(t)$  is thermal noise from random molecular collisions
- $F_{ext}(t)$  is any external force we might apply

The FDT connects two important quantities:

1. The **position autocorrelation function**  $C(t-t')$ , which tells us how the particle's random motions are correlated across time:

$$C(t-t') = \langle x(t)x(t') \rangle - \langle x(t) \rangle \langle x(t') \rangle$$

In equilibrium with no external force, this equals:

$$C(t-t') = \frac{k_B T}{k} e^{-\frac{k}{\gamma}|t-t'|}$$

2. The **response function**  $\chi(t-t')$ , which measures how the particle's position responds to a small external force:

$$\chi(t-t') = \frac{\delta \langle x(t) \rangle}{\delta F_{ext}(t')}$$

For our harmonic trap:

$$\chi(t-t') = \frac{1}{\gamma} e^{-\frac{k}{\gamma}(t-t')} \Theta(t-t')$$

where  $\Theta(t-t')$  is the Heaviside step function (ensuring causality - the system can't respond before the force is applied).

The FDT directly relates these quantities through temperature:

$$\chi(t-t') = -\frac{1}{k_B T} \frac{d}{dt} C(t-t') \quad \text{for } t > t'$$

This equation embodies the profound insight that the same microscopic mechanisms responsible for dissipation (friction) also generate fluctuations, with temperature determining their relative strength.

The FDT is a powerful tool in equilibrium systems, but it breaks down in active matter. In active systems, energy is continuously injected at the microscopic level through self-propulsion mechanisms. This additional energy input means that fluctuations can be much larger than what would be predicted from the system's response properties using the equilibrium FDT.

The violation of the FDT in active systems provides a quantitative measure of how far these systems operate from equilibrium, making it a valuable tool for characterizing active matter.

### 4.3 Examples

#### Two Brownian particles with non-uniform temperatures

To concretely illustrate how equilibrium concepts apply to coupled systems and how they break down when thermal equilibrium is violated, let's consider a simple model: two Brownian particles connected by springs, with different temperatures.

Consider the following system: - Two Brownian particles with positions  $x_1$  and  $x_2$  - Particle 1 is connected to a fixed wall by a spring with constant  $k_1$  - The two particles are connected to each other by a spring with constant  $k_2$  - Particle 2 is connected to a fixed wall by a spring with constant  $k_3$  - Particle 1 experiences thermal fluctuations at temperature  $T_1$  - Particle 2 experiences thermal fluctuations at temperature  $T_2$

The Langevin equations for this system are:

$$\begin{aligned}\gamma_1 \frac{dx_1}{dt} &= -k_1 x_1 - k_2(x_1 - x_2) + \xi_1(t) \\ \gamma_2 \frac{dx_2}{dt} &= -k_3 x_2 - k_2(x_2 - x_1) + \xi_2(t)\end{aligned}$$

where  $\gamma_i$  are the friction coefficients and  $\xi_i(t)$  are Gaussian white noises with:

$$\langle \xi_i(t) \rangle = 0, \quad \langle \xi_i(t) \xi_i(t') \rangle = 2\gamma_i k_B T_i \delta(t - t')$$

When  $T_1 = T_2$ , this system is in thermal equilibrium, and the probability distribution for the positions follows the Boltzmann distribution:

$$P(x_1, x_2) \propto \exp\left(-\frac{1}{k_B T} [k_1 x_1^2 / 2 + k_2 (x_1 - x_2)^2 / 2 + k_3 x_2^2 / 2]\right)$$

However, when  $T_1 \neq T_2$ , the system is driven out of equilibrium, leading to a non-Boltzmann stationary distribution. The correlation between  $x_1$  and  $x_2$  encodes information about the non-equilibrium nature of the system.

In this non-equilibrium scenario, energy flows from the hotter to the colder particle, driving the system away from equilibrium. The stationary state represents a balance between this energy flow and dissipation, rather than a state of maximum entropy as in equilibrium systems. The detailed balance condition is violated, and the system exhibits persistent probability currents in phase space - a hallmark of non-equilibrium behavior.

#### Chlamydomonas Swimming

The violation of detailed balance is perhaps the most direct signature of non-equilibrium behavior in active matter. The microalgae Chlamydomonas Reinhardtii provides an exemplary demonstration of this principle.

Chlamydomonas Reinhardtii propels itself through fluid by coordinated beating of its two flagella. This motion requires continuous energy consumption, as each flagellum hydrolyzes ATP to power molecular motors that generate rhythmic beating patterns. Unlike passive Brownian particles, where motion arises from random thermal fluctuations, the flagellar beating represents a driven, non-equilibrium process.

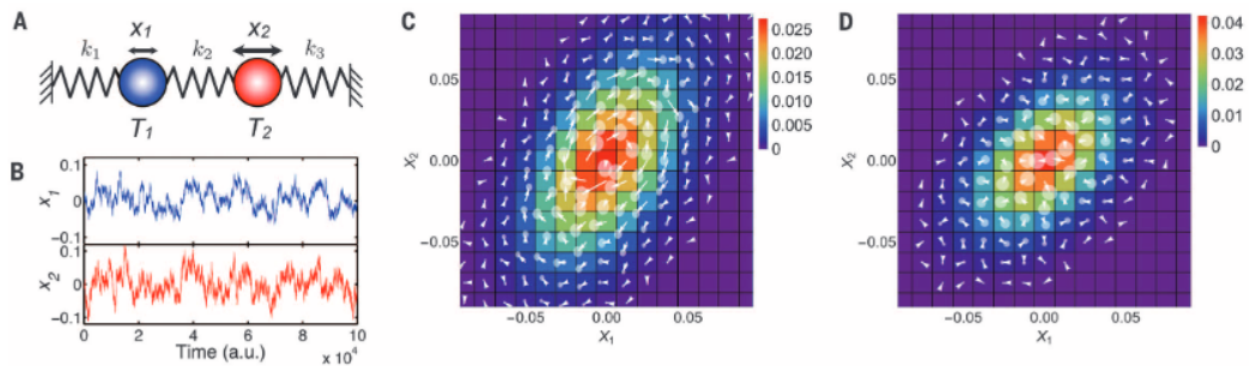


Figure 4.3: Brownian-dynamics simulation of 1D bead-spring model. (A) Model schematic. (B) Time series of the bead positions for T<sub>2</sub> = 1.5T<sub>1</sub> and equal spring constants. See figs. S4 and S5 for the general case (18). (C and D) Probability distribution (color) and flux map (white arrows) in CGPS spanned by x<sub>1</sub> and x<sub>2</sub> for the simulation in panel B (C) and for a simulation with T<sub>2</sub> = T<sub>1</sub> (D). Translucent disks represent a 2s confidence interval for fluxes. [source](#)



Figure 4.4: Light microscopy image of Chlamydomonas Reinhardtii, a single-celled green alga with two flagella used for swimming and sensing. [source](#)

As shown in the figures below, researchers have characterized this non-equilibrium behavior by analyzing the flagellar dynamics in a coarse-grained phase space (CGPS) constructed from the principal bending modes. The beating patterns can be decomposed into these fundamental modes (similar to Fourier components), allowing quantitative tracking of the flagellar configuration over time.

The phase space probability distribution and corresponding flux maps reveal a striking signature of non-equilibrium dynamics: coherent probability currents that form closed loops. These directed cyclic trajectories through configuration space explicitly violate detailed balance, which would require all microscopic transitions to be pairwise-balanced with no net probability flux between states. In an equilibrium system, transitions between any two states would occur with equal frequency in both directions when properly weighted by their equilibrium probabilities.

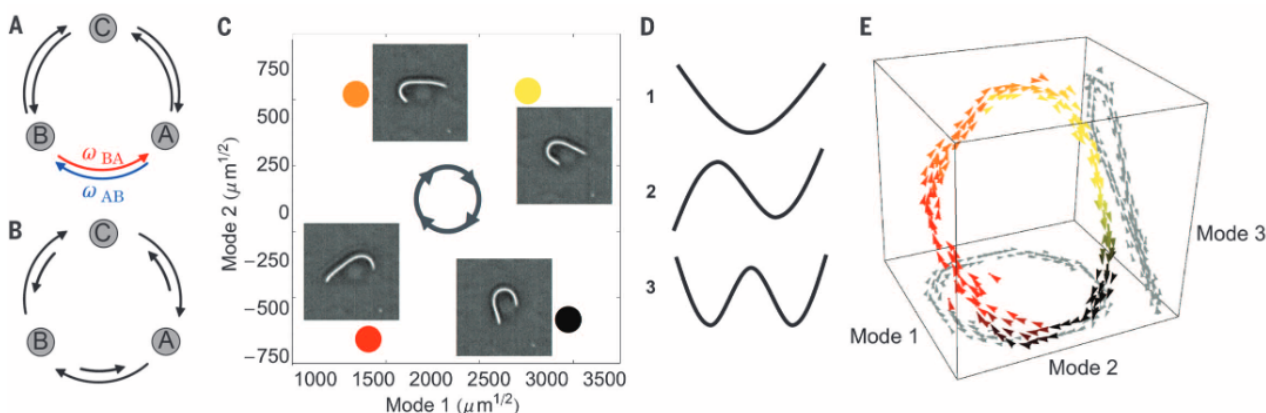


Figure 4.5: Detailed balance and actively beating Chlamydomonas flagella. (A) In thermodynamic equilibrium, transitions between microscopic states are pairwise-balanced, precluding net flux among states. (B) Nonequilibrium steady states can break detailed balance and exhibit flux loops. (C) Snapshots separated by 24 (orange-yellow), 7, and 10 ms in an isolated Chlamydomonas flagellum's beat cycle (movie S1). Arrows on the central circle indicate the direction of time. Color corresponds to position in (E). (D) The first three bending modes for a freely suspended flexible rod. (E) A three-dimensional (3D) probability flux map of flagellar dynamics in the CGPS spanned by the first three modes.[source](#)

The flux maps in panels F and G below show clear rotational currents in the phase space of bending modes. These currents represent the flagellum cycling through configurations in a specific sequence rather than randomly exploring available states as would occur in thermal equilibrium. The directed nature of these probability currents directly quantifies the system's departure from equilibrium.

These probability flux loops are fundamental to biological function, enabling directed motion and mechanical work that would be thermodynamically prohibited under equilibrium constraints. Similar non-equilibrium dynamics appear in many biological systems, from molecular motors and cell migration to collective tissue behaviors, where energy consumption drives the system away from equilibrium to perform essential biological functions.

### Primary cilia in epithelial cells

Primary cilia represent another biological system that exhibits non-equilibrium dynamics, but in a more subtle manner than the flagella of Chlamydomonas. These hairlike organelles project from many eukaryotic cells and transduce mechanical and chemical stimuli into intracellular signals. Unlike flagella, primary cilia often lack the dynein machinery necessary for active beating, causing them to fluctuate in what appears to be a random manner.

When analyzed in the phase space defined by their deflection angle and curvature, primary cilia of MDCK (Madin-Darby canine kidney) epithelial cells reveal clockwise circulation patterns in their probability flux maps. These patterns indicate broken detailed balance, providing direct evidence of non-equilibrium dynamics in these seemingly passive structures. The statistical significance of these flux loops can be quantified, confirming that these cilia indeed operate far from equilibrium despite their apparently random motion.

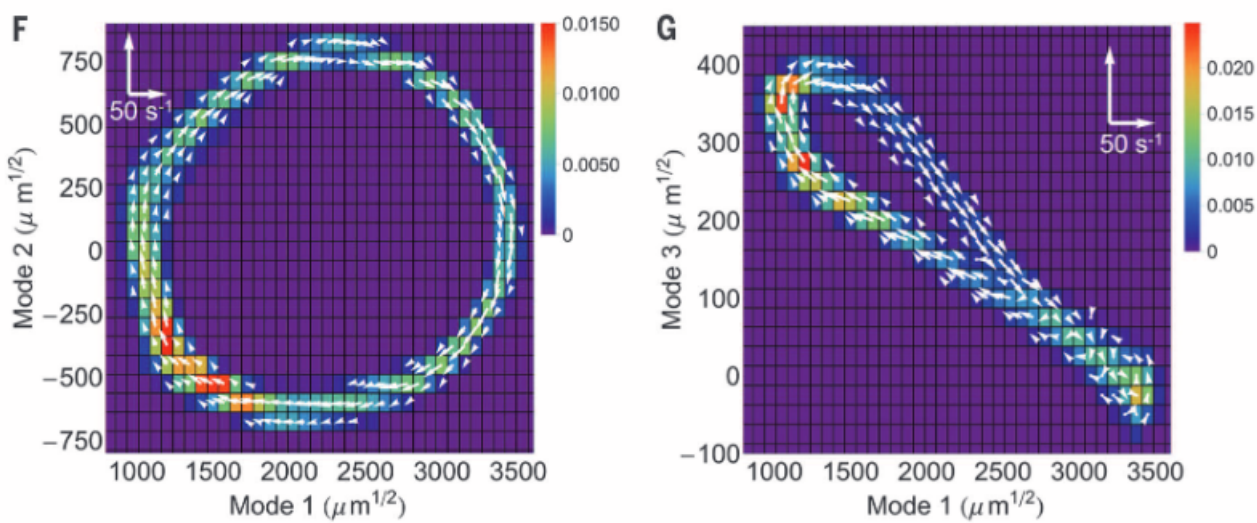


Figure 4.6: (F and G) Probability distribution (color) and flux map (white arrows) of flagellar dynamics in CGPS spanned by first and second modes (F), and first and third modes (G). The white legend indicates the flux scale. [source](#)

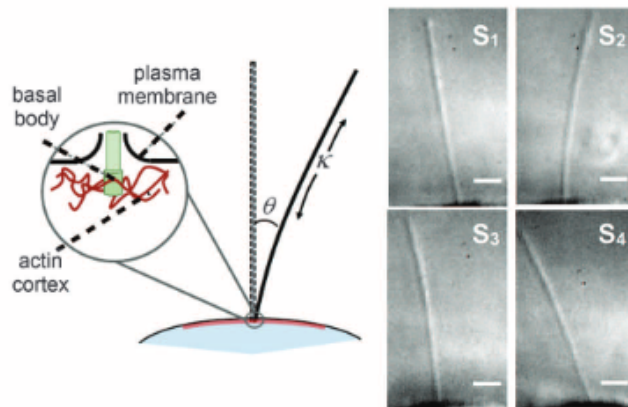


Figure 4.7: Left: Schematic of primary cilium and anchoring of the basal body in the cell cortex with angle  $\theta$  and curvature,  $\kappa$ , defined positive as shown. Right: Snapshots of cilium, from differential interference contrast microscopy, taken at time points marked in (B). Scale bar: 2 mm.



# Chapter 5

# Microscopic Models of Self-propulsion

## 5.1 Introduction: From Equilibrium Violations to Microscopic Models

In the previous lecture, we explored the fundamental concepts of equilibrium statistical mechanics and how active biological systems violate these principles. We examined detailed balance and the fluctuation-dissipation theorem (FDT), discovering that active systems consistently break these equilibrium constraints.

One of the key examples we studied was sedimentation, where colloidal particles in thermal equilibrium form an exponential density profile according to the Boltzmann distribution:

$$n(h) = n_0 e^{-\frac{mgh}{k_B T}}$$

This distribution arises directly from equilibrium statistical mechanics and represents a balance between gravitational forces and thermal fluctuations.

But what happens when particles are active - consuming energy to propel themselves? This lecture begins by exploring one of the simplest active matter models: the run-and-tumble particle (RTP). We'll first examine this model in 1D with sedimentation to directly contrast with our equilibrium example from lecture 2, demonstrating how active particles violate equilibrium principles even in this simplified scenario.

From there, we'll extend to more sophisticated microscopic models that can capture the essential features of self-propelled particles in three dimensions:

1. **Run-and-Tumble Particles (RTPs)** - inspired by bacterial motion patterns like E. coli
2. **Active Brownian Particles (ABPs)** - which combine random diffusion with persistent self-propulsion
3. **Swimming at Low Reynolds Number** - examining the physics that governs locomotion at the microscale
4. **Hydrodynamic Interactions** - understanding how active particles influence their surroundings and each other
5. **Microswimmer Force Dipoles** - characterizing the flow fields generated by different types of swimmers

These models will provide us with the tools to analyze collective behaviors, pattern formation, and non-equilibrium dynamics in active biological systems.

## 5.2 Run-and-Tumble Particles (RTPs)

Run-and-tumble dynamics represent an important class of active motion, inspired by the swimming behavior of bacteria like E. coli. Unlike passive Brownian motion, run-and-tumble particles alternate between straight-line “runs” and random reorientation “tumbles.”

This run-and-tumble motion, which comes in different flavors (e.g. a run-and reverse motion as displayed in the movie above) has even some functionality. It allows bacteria to move in gradients of chemical species concentrations without measuring even the gradient directly.

## 1D Run-and-Tumble with Sedimentation

We can make a simple model for this run-and-tumble motion in one dimension. Let's start with the master equations for the probabilities  $P_+(x, t)$  and  $P_-(x, t)$  of finding a particle at position  $x$  moving in the positive or negative direction, respectively. In the simplest case without gravity or diffusion:

$$\frac{\partial P_+}{\partial t} = -\frac{\partial}{\partial x}(v_0(x)P_+) - \lambda P_+ + \lambda P_-$$

$$\frac{\partial P_-}{\partial t} = \frac{\partial}{\partial x}(v_0(x)P_-) + \lambda P_+ - \lambda P_-$$

These equations describe how probabilities change due to advection at position-dependent speed  $v_0(x)$  and flipping of the swimming direction with rate  $\lambda$ .

We can rewrite these equations in terms of the total probability density  $P(x, t) = P_+(x, t) + P_-(x, t)$  and the polarization  $\sigma(x, t) = P_+(x, t) - P_-(x, t)$ . After adding and subtracting the equations:

$$\frac{\partial P}{\partial t} = -\frac{\partial}{\partial x}(v_0(x)\sigma)$$

$$\frac{\partial \sigma}{\partial t} = -\frac{\partial}{\partial x}(v_0(x)P) - 2\lambda\sigma$$

### Note

From the first equation, we can identify the probability current as  $J(x, t) = v_0(x)\sigma(x, t)$ . In the steady state,  $\frac{\partial \sigma}{\partial t} = 0$ , which gives:

$$\frac{\partial}{\partial x}(v_0(x)P) = -2\lambda\sigma$$

$$v_0(x)\frac{\partial P}{\partial x} + P\frac{dv_0(x)}{dx} = -2\lambda\sigma$$

Solving for  $\sigma$ :

$$\sigma(x) = -\frac{v_0(x)}{2\lambda}\frac{\partial P}{\partial x} - \frac{P}{2\lambda}\frac{dv_0(x)}{dx}$$

This then yields the current:

$$J(x) = v_0(x)\sigma(x) = -\frac{v_0^2(x)}{2\lambda}\frac{\partial P}{\partial x} - \frac{v_0(x)P}{2\lambda}\frac{dv_0(x)}{dx}$$

This has the form of a drift-diffusion current  $J = -D_{\text{eff}}\frac{\partial P}{\partial x} + V_{\text{eff}}P$  with a position-dependent effective diffusion coefficient  $D_{\text{eff}}(x) = \frac{v_0^2(x)}{2\lambda}$  and an effective drift velocity  $V_{\text{eff}}(x) = -\frac{v_0(x)P}{2\lambda}\frac{dv_0(x)}{dx}$ .

### Density Distributions in Different Regimes

One can find out now the steady state distribution of run-and-tumble swimmers for different cases. Two interesting ones are:

- 1) **Position-dependent tumble rate, constant speed:** When the speed  $v_0$  is constant but the tumble rate  $\lambda(x)$  varies with position, the steady-state current is:

$$J(x) = -\frac{v_0^2}{2\lambda(x)} \frac{\partial P}{\partial x}$$

Setting  $J(x) = 0$  for the steady state yields:

$$\frac{\partial P}{\partial x} = 0$$

This gives a uniform density distribution:

$$P(x) = \text{constant}$$

Interestingly, spatial variation in tumble rate alone ( $\lambda(x)$ ) cannot create population gradients when the swimming speed is constant. However, in bacterial chemotaxis, the tumble rate depends not just on position but also on the bacterium's orientation relative to the chemical gradient:  $\lambda(\mathbf{r}, \mathbf{n}) = \lambda_0(1 - \mathbf{n} \cdot \nabla c(\mathbf{r})/|\nabla c(\mathbf{r})|)$ . This directional dependence allows bacteria to effectively navigate chemical landscapes, creating population gradients despite constant swimming speed. (see for example 1)

#### Chemotaxis

Chemotaxis is the directed movement of organisms in response to chemical gradients in their environment. This behavior allows cells to move toward favorable chemical conditions (positive chemotaxis) or away from harmful ones (negative chemotaxis). In bacteria like E. coli, chemotaxis works through a biased random walk: rather than directly sensing gradient directions, bacteria adjust their tumbling frequency based on whether they're moving toward or away from attractive chemicals. This elegant mechanism enables even simple single-celled organisms to effectively navigate complex chemical landscapes without sophisticated sensory apparatus.

- 2) **Position-dependent speed, constant tumble rate:** When the swimming speed depends on position  $v_0(x)$  while the tumble rate  $\lambda$  remains constant, we can find the steady-state density distribution by setting  $J(x) = 0$  (no flux condition) and solving:

$$-\frac{v_0^2(x)}{2\lambda} \frac{\partial P}{\partial x} - \frac{v_0(x)P}{2\lambda} \frac{dv_0(x)}{dx} = 0$$

This simplifies to:

$$\frac{\partial P}{\partial x} = -\frac{1}{v_0(x)} \frac{dv_0(x)}{dx} P$$

The solution gives the steady-state density distribution:

$$P(x) \propto \frac{1}{v_0(x)}$$

This reveals that bacteria naturally accumulate in regions of lower swimming speed. Looking at the effective drift velocity  $V_{\text{eff}}(x) = -\frac{v_0(x)}{2\lambda} \frac{dv_0(x)}{dx} = -\frac{1}{4\lambda} \frac{d(v_0^2(x))}{dx}$ , we see bacteria will move toward regions where swimming speed decreases. This provides a mechanism for chemotaxis without directly modulating the tumbling rate. In fact this overwrites the detailed balance equation we obtained earlier for equilibrium.

### Sedimentation of Run-and-tumble particles

With a little bit of effort, one can modify this simple model to include an additional sedimentation drift velocity which is given by  $mg/\gamma$ , where  $\gamma$  is the friction coefficient. Including further thermal diffusion yields:

$$\frac{\partial P_+}{\partial t} = -\frac{\partial}{\partial x} \left[ (v_0(x) - \frac{mg}{\gamma}) P_+ \right] - \lambda P_+ + \lambda P_- + D \frac{\partial^2 P_+}{\partial x^2}$$

$$\frac{\partial P_-}{\partial t} = -\frac{\partial}{\partial x} \left[ (-v_0(x) - \frac{mg}{\gamma}) P_- \right] + \lambda P_+ - \lambda P_- + D \frac{\partial^2 P_-}{\partial x^2}$$

In the steady state, when thermal diffusion is small ( $D \approx 0$ ), we obtain:

$$P(x) = P_+(x) + P_-(x) \propto e^{-\frac{x}{\delta}}$$

where  $\delta$  is the sedimentation length

$$\delta = \frac{v_0^2 - (mg/\gamma)^2}{2\lambda mg/\gamma}$$

This is strikingly different from the equilibrium result! When sedimentation speed and active particle speed are comparable the sedimentation length is zero. The bacteria would completely collapse to a layer on the surface.

If the speed is now bigger than the sedimentation speed, the sedimentation length becomes positive.

Since the sedimentation length in equilibrium is

$$\delta = \frac{k_B T}{mg}$$

it is tempting to say that

$$\frac{k_B T_{\text{eff}}}{mg} = \frac{v_0^2 - (mg/\gamma)^2}{2\lambda mg/\gamma}$$

which yields an effective temperature

$$T_{\text{eff}} = \frac{v_0^2 - (mg/\gamma)^2}{2\lambda k_B}$$

which is not the temperature of the surrounding medium. This effective temperature accounts for the active motion of the particle and its interaction with the surrounding medium.

```
# Parameters
x = np.linspace(0, 10, 1000) # height above surface
v_sed = 1 # sedimentation velocity mg/
lambda_tumble = 0.6 # tumble rate

# Three different active velocities
v0_values = [1.01, 2, 3] # self-propulsion speeds

# Calculate density profiles
plt.figure(figsize=get_size(10, 8))

for v0 in v0_values:
    # Calculate sedimentation length
```

```

delta = (v0**2 - v_sed**2) / (2 * lambda_tumble * v_sed)

density = np.exp(-x / delta)

density = density / density[0]

plt.plot(x, density, '--', linewidth=1, label=f'${v_0} = {v0}$')

plt.xlabel('height $z$')
plt.ylabel('$P(x)/P(0)$')
plt.legend()
plt.tight_layout()
plt.show()

```

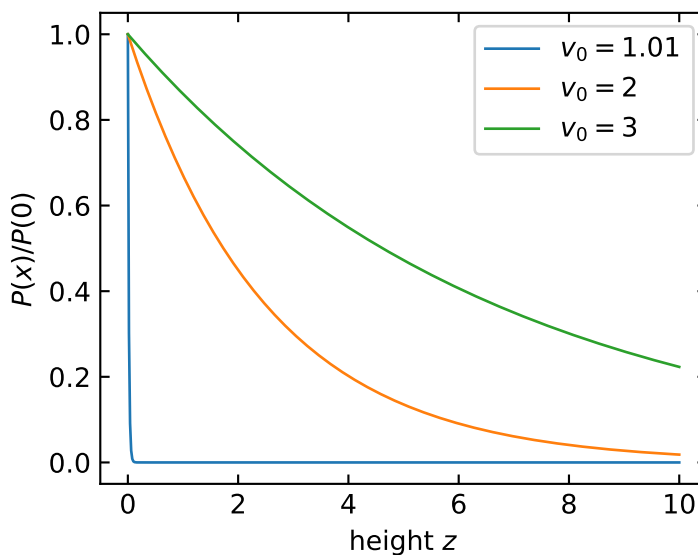


Figure 5.1: Sedimentation profiles for three different activity levels. As the speed  $v_0$  increases relative to the sedimentation velocity  $mg/\gamma = 1$ , the density profile extends further from the bottom surface.

## Mathematical Formulation in Higher Dimensions

Extending to higher dimensions, the equations of motion for a run-and-tumble particle can be written as:

$$\frac{d\mathbf{r}}{dt} = v_0 \mathbf{n}(t) - \frac{1}{\gamma} \nabla U(\mathbf{r}) + \xi(t)/\gamma$$

where  $\mathbf{n}(t)$  represents the orientation vector that changes discontinuously according to a Poisson process. This stochastic process models tumbling events as memory-less, random occurrences with the fundamental property:

$$P(\text{tumble in interval } [t, t+dt]) = \lambda dt + o(dt)$$

where  $\lambda$  is the tumbling rate and  $o(dt)$  represents higher-order terms that become negligible for small  $dt$ . This formulation has several important implications:

1. The probability of a tumble occurring in any small time interval  $dt$  is proportional to the length of that interval, with  $\lambda$  being the proportionality constant.
2. Tumbling events are statistically independent - the probability of a tumble occurring is unaffected by when the previous tumble occurred, giving the process its “memory-less” property.

3. The waiting times between consecutive tumbles follow an exponential distribution with mean  $1/\lambda$ :

$$P(\text{time between tumbles} > \tau) = e^{-\lambda\tau}$$

4. The number of tumbles  $N(t)$  occurring within a time interval  $[0, t]$  follows a Poisson distribution:

$$P(N(t) = k) = \frac{(\lambda t)^k e^{-\lambda t}}{k!}$$

A critical aspect of the run-and-tumble model is how the new orientation is determined after each tumbling event. In the standard model, the new orientation vector  $\mathbf{n}(t^+)$  immediately after a tumble at time  $t$  is chosen from a uniform probability distribution on the unit circle (in 2D) or sphere (in 3D), completely independent of the previous orientation  $\mathbf{n}(t^-)$ . This means:

- In 2D: The new angle  $\theta_{new}$  is drawn uniformly from  $[0, 2\pi)$
- In 3D: The new direction is uniformly distributed on the unit sphere, typically generated by choosing  $\phi$  uniformly from  $[0, 2\pi)$  and  $\cos\theta$  uniformly from  $[-1, 1]$

This uniform reorientation distribution is a key feature that distinguishes run-and-tumble motion from other active particle models. For some biological swimmers, variations of this distribution may be more appropriate - for example, some bacteria exhibit a “persistence” in their tumbling, where the new direction maintains some correlation with the previous direction. Other organisms might show “run-and-reverse” behavior, where the new orientation is preferentially opposite to the previous one. These variations can be modeled by modifying the reorientation distribution accordingly.

```
# Parameters for run-and-tumble motion
v0 = 1.0          # speed (constant)
lambda_tumble = 0.4 # tumble rate
total_time = 50    # total simulation time
dt = 0.1          # time step

# Function to generate a single run-and-tumble trajectory
def simulate_run_tumble_2d(v0, lambda_tumble, total_time, dt, seed=None):
    if seed is not None:
        np.random.seed(seed)

    # Number of time steps
    n_steps = int(total_time / dt)

    # Initialize arrays for position and orientation
    x = np.zeros(n_steps)
    y = np.zeros(n_steps)
    theta = np.zeros(n_steps)

    # Set random initial orientation
    theta[0] = 2 * np.pi * np.random.random()

    # Simulate run-and-tumble motion
    for i in range(1, n_steps):
        # Check if tumble occurs (Poisson process)
        if np.random.random() < lambda_tumble * dt:
            # New random orientation
            theta[i] = 2 * np.pi * np.random.random()
        else:
            # Keep same orientation
            theta[i] = theta[i-1]

    # Update position
```

```

x[i] = x[i-1] + v0 * np.cos(theta[i]) * dt
y[i] = y[i-1] + v0 * np.sin(theta[i]) * dt

return x, y

# Create figure
plt.figure(figsize=get_size(10, 10))

# Generate and plot 10 trajectories
for i in range(10):
    x, y = simulate_run_tumble_2d(v0, lambda_tumble, total_time, dt, seed=i)
    plt.plot(x, y, '-', linewidth=1, alpha=0.7)

# Add marker for starting point
plt.scatter(0, 0, color='red', s=50)

plt.xlabel('x')
plt.ylabel('y')
plt.axis('equal')
plt.grid(True, linestyle='--', alpha=0.3)
plt.xlim(-15, 15)
plt.ylim(-15, 15)
plt.tight_layout()
plt.show()

```

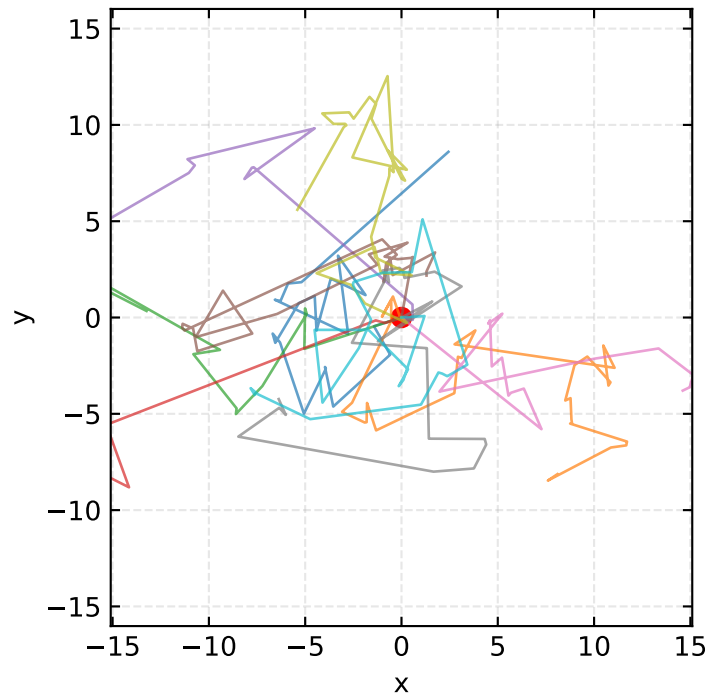


Figure 5.2: Ten trajectories of run-and-tumble particles in 2D, each starting from the origin. The particles move with constant speed  $v = 1$  and randomly change direction according to a Poisson process with rate  $\lambda = 0.1$ .

### Connection to ABPs

Interestingly, in the limit of long observation times, the large-scale dynamics of RTPs become equivalent to those of ABPs. The effective rotational diffusion coefficient for RTPs is:

$$D_r^{\text{eff}} = \frac{\lambda}{d-1}$$

where  $d$  is the dimensionality. This equivalence suggests that these seemingly different microscopic mechanisms can lead to similar macroscopic behaviors.

## Non-equilibrium Aspects

RTP models demonstrate several non-equilibrium features beyond the effective temperature we observed in sedimentation:

1. The steady-state cannot be written as a Boltzmann distribution
2. Probability currents exist even in steady state
3. The fluctuation-dissipation theorem is violated

These features arise from the persistent energy consumption required to maintain the run-and-tumble motion.

## 5.3 Active Brownian Particles (ABPs)

After examining Run-and-Tumble Particles, we now turn to Active Brownian Particles (ABPs), which represent another fundamental model of self-propelled agents. Like RTPs, ABPs extend the equilibrium Brownian motion framework we discussed in Lecture 2, but they do so through continuous rotational diffusion rather than discrete tumbling events. This alternative self-propulsion mechanism similarly drives the system out of equilibrium.

### Mathematical Formulation

To understand Active Brownian Particles, we should start from the general underdamped Langevin equation for Brownian motion:

$$m \frac{d^2\mathbf{r}}{dt^2} = \underbrace{-\gamma \frac{d\mathbf{r}}{dt}}_{\text{sink}} - \nabla U(\mathbf{r}) + \underbrace{\xi(t)}_{\text{source}}$$

Here,  $\mathbf{r} = (x, y)$  is the particle position,  $m$  is the particle mass, and the left side represents inertial forces. On the right side we have a dissipative friction term with coefficient  $\gamma$  that removes energy from the system, a conservative force from the potential  $U(\mathbf{r})$ , and a thermal noise term  $\xi(t)$  that injects energy into the particle motion. The thermal translational noise  $\xi(t)$  has zero mean ( $\langle \xi(t) \rangle = 0$ ) and correlations  $\langle \xi_i(t) \xi_j(t') \rangle = 2\gamma k_B T \delta_{ij} \delta(t-t')$ , following the fluctuation-dissipation theorem.

The energy dissipation rate due to friction is given by  $P_{diss} = \gamma |\mathbf{v}|^2$ , where  $\mathbf{v} = \frac{d\mathbf{r}}{dt}$  is the particle velocity. In equilibrium, the average energy dissipation rate per degree of freedom is  $\langle P_{diss} \rangle = \frac{2\gamma k_B T}{m}$ . Meanwhile, the energy injection rate from thermal fluctuations is  $P_{inj} = \xi(t) \cdot \mathbf{v}$ , with an average value of  $\langle P_{inj} \rangle = \frac{2\gamma k_B T}{m}$  per degree of freedom. The equality between these rates ensures detailed balance in equilibrium systems, maintaining a consistent average kinetic energy of  $\frac{k_B T}{2}$  per degree of freedom in accordance with the equipartition theorem.

For microscopic particles in a viscous medium, the inertial term becomes negligible (mass effects disappear on timescales  $t \gg m/\gamma$ ), leading to the overdamped limit.

In an ABP, we add a non-equilibrium self-propulsion force, resulting in these overdamped Langevin equations:

$$\gamma \frac{d\mathbf{r}}{dt} = \gamma v_0 \mathbf{n}(t) - \nabla U(\mathbf{r}) + \xi(t)$$

$$\frac{d\theta}{dt} = \eta(t)$$

The first equation describes the particle's translational motion, where  $v_0$  is the self-propulsion speed and  $\mathbf{n}(t) = (\cos \theta(t), \sin \theta(t))$  is a unit vector pointing in the direction of self-propulsion.

The second equation governs the particle's orientation  $\theta$ , which evolves through rotational diffusion. The rotational noise  $\eta(t)$  has zero mean ( $\langle \eta(t) \rangle = 0$ ) and correlations  $\langle \eta(t)\eta(t') \rangle = 2D_r\delta(t-t')$ , where  $D_r$  is the rotational diffusion coefficient.

Unlike passive Brownian motion discussed in Lecture 2, ABPs fundamentally violate detailed balance due to the persistent self-propulsion term, which acts as an additional energy source driving the system out of equilibrium. The particle moves with a characteristic persistence time  $\tau_r = 1/D_r$  before its direction is randomized by rotational diffusion.

## Mean Displacement

If we consider an active Brownian particle in two dimension starting at the origin ( $x=0, y=0$ ) with an initial orientation  $=0$  (pointing along the positive x-axis), the mean displacement shows interesting directional behavior:

$$\langle x(t) \rangle = \frac{v_0}{D_r} (1 - e^{-D_r t})$$

$$\langle y(t) \rangle = 0$$

The mean displacement in the y-direction averages to zero due to the symmetry of rotational diffusion. The x-component shows an initial ballistic growth that saturates at the persistence length scale  $l_p = v_0/D_r$  for times much larger than the rotational diffusion time  $\tau_r = 1/D_r$ . This persistence length represents the typical distance traveled before the particle's direction is randomized.

Unlike equilibrium Brownian motion where the mean displacement is zero in all directions, the ABP's mean displacement reflects the persistence of its self-propulsion. As  $t \rightarrow \infty$ , the orientation becomes fully randomized, and any further displacement averages to zero, resulting in the saturation of the mean displacement to a finite value.

6.067852395301331

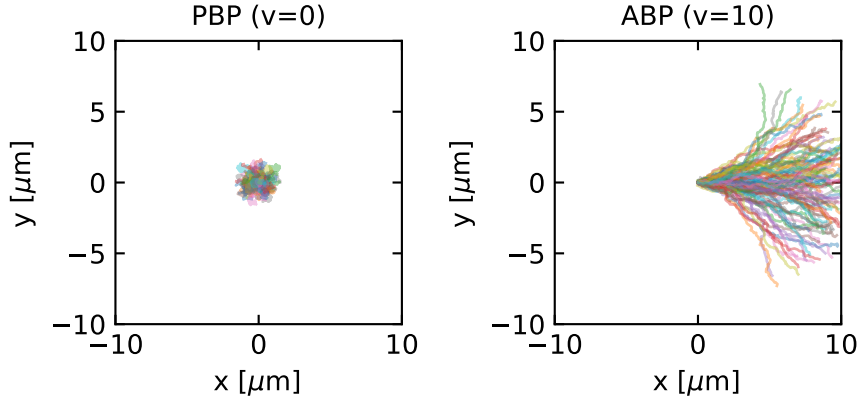


Figure 5.3: Trajectories of a particle ( $R=1 \mu\text{m}$ ) starting at the origin with an initial orientation  $\theta = 0$ . Left: Passive Brownian Particle ( $v = 0 \mu\text{m}/\text{s}$ ). Right: Active Brownian Particle ( $v = 10 \mu\text{m}/\text{s}$ ). ( $\tau_r = 6\text{s.}$ )

## Mean Square Displacement

The mean square displacement (MSD) of an ABP reveals a rich multi-regime behavior that can be analyzed from the full expression:

$$\langle |\mathbf{r}(t) - \mathbf{r}(0)|^2 \rangle = 4D_t t + \frac{2v_0^2}{D_r^2} (D_r t - 1 + e^{-D_r t})$$

where  $D_t = k_B T / \gamma$  is the thermal translational diffusion coefficient.

We can identify three distinct regimes by examining the limiting behavior at different timescales:

1. **Very short times** ( $t \ll \tau_r$ , where  $\tau_r = 1/D_r$  is the rotational diffusion time):

By expanding the exponential term  $e^{-D_r t} \approx 1 - D_r t + \frac{(D_r t)^2}{2} - \dots$ , we obtain:

$$\langle |\mathbf{r}(t) - \mathbf{r}(0)|^2 \rangle \approx 4D_t t + v_0^2 t^2 + \dots$$

This reveals a combination of diffusive behavior ( $\sim t$ ) from thermal fluctuations and the beginning of ballistic motion ( $\sim t^2$ ) from persistent self-propulsion.

2. **Intermediate times** ( $\tau_t \ll t \ll \tau_r$ ):

The ballistic term dominates and the MSD scales approximately as:

$$\langle |\mathbf{r}(t) - \mathbf{r}(0)|^2 \rangle \approx v_0^2 t^2$$

This quadratic scaling reflects the persistent directed motion before rotational diffusion randomizes the swimming direction.

3. **Long times** ( $t \gg \tau_r$ ):

When  $t \gg 1/D_r$ ,  $e^{-D_r t} \approx 0$ , and the MSD becomes:

$$\langle |\mathbf{r}(t) - \mathbf{r}(0)|^2 \rangle \approx 4D_t t + \frac{2v_0^2}{D_r} t - \frac{2v_0^2}{D_r^2}$$

For sufficiently long times, the constant term becomes negligible, resulting in diffusive motion with an enhanced effective diffusion coefficient:

$$D_{\text{eff}} = D_t + \frac{v_0^2}{2dD_r}$$

where  $d$  is the dimensionality. This enhanced diffusion coefficient represents a key signature of the system's non-equilibrium nature and cannot be explained by equilibrium statistical mechanics.

```
# Parameters
D_t = 1.0      # thermal translational diffusion coefficient
v_0 = 5.0      # self-propulsion speed
D_r = 0.2      # rotational diffusion coefficient
tau_r = 1/D_r  # rotational diffusion time

# Calculate theoretical MSD
def msd_theory(t, D_t, v_0, D_r):
    """Theoretical mean square displacement for active Brownian particles"""
    return 4*D_t*t + (2*v_0**2)/(D_r**2)*(D_r*t - 1 + np.exp(-D_r*t))

# Time range spanning multiple regimes
t = np.logspace(-2, 2, 1000)  # from 0.01 to 100
msd = msd_theory(t, D_t, v_0, D_r)

# Calculate effective diffusion coefficient
```

```

D_eff = D_t + v_0**2/(2*D_r)

# Create figure
plt.figure(figsize=get_size(10, 8))

# Plot MSD on log-log scale
plt.loglog(t, msd, 'b-', linewidth=2, label='MSD of ABP')

# Add reference lines for different scaling regimes
t_ref = np.array([0.05, 50])
plt.loglog(t_ref, 4*D_t*t_ref, 'k--', label=r'$\sim 4D_t t$ (thermal diffusion)')
plt.loglog(t_ref, v_0**2*t_ref**2, 'r--', label=r'$\sim v_0^2 t^2$ (ballistic)')
plt.loglog(t_ref, 4*D_eff*t_ref, 'g--', label=r'$\sim 4D_{eff}t$ (enhanced diffusion)')

# Add vertical line at rotational diffusion time
plt.axvline(x=tau_r, color='gray', linestyle=':', label=r'$\tau_r = 1/D_r$')

# Mark the three regimes
#plt.annotate("Short-time regime", xy=(0.02, 0.3), xytext=(0.02, 0.3), fontsize=9)
#plt.annotate("Intermediate-time regime", xy=(0.5, 10), xytext=(0.5, 10), fontsize=9)
#plt.annotate("Long-time regime", xy=(10, 200), xytext=(10, 200), fontsize=9)

plt.xlabel(r'Time $t$')
plt.ylabel(r'MSD $\langle |\mathbf{r}(t) - \mathbf{r}(0)|^2 \rangle$')
# plt.legend()
plt.tight_layout()
plt.show()

```

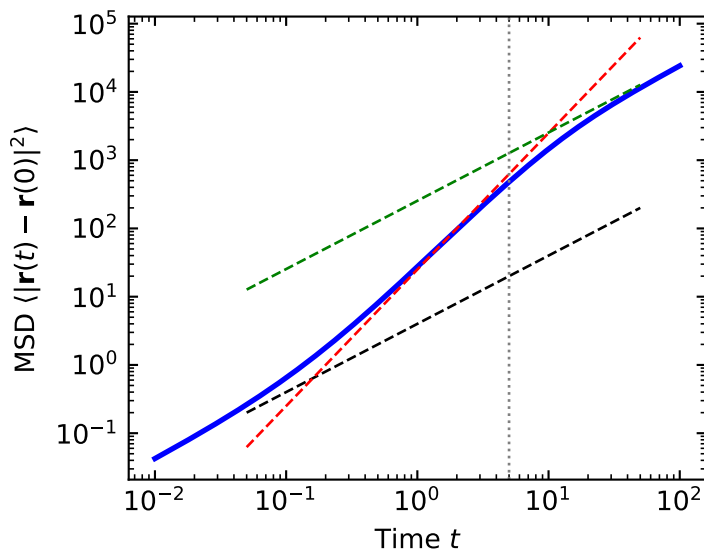


Figure 5.4: Mean square displacement (MSD) of an active Brownian particle showing three distinct regimes. At short times ( $t \ll \tau_r$ ), a combination of diffusive and ballistic motion is observed. At intermediate times, ballistic motion dominates ( $\text{MSD} \sim t^2$ ). At long times ( $t \gg \tau_r$ ), enhanced diffusion emerges with an effective diffusion coefficient larger than the thermal value.

## Probability Distribution

The steady-state probability distribution of ABPs cannot be written in the Boltzmann form, unlike equilibrium systems. Instead, it depends on both position and orientation, and generally has to be obtained numerically or through approximation methods.

In homogeneous space, the orientation-averaged probability distribution is uniform. However, in the presence of boundaries or spatially varying potentials, ABPs exhibit phenomena like accumulation at surfaces and trapping in local potential minima that are qualitatively different from equilibrium Brownian particles.

## Time Reversal Symmetry Breaking

One of the hallmarks of equilibrium systems is their invariance under time reversal. For passive Brownian particles, if we were to watch a movie of particle motion and then play it backwards, the reversed trajectories would still be physically plausible and consistent with the laws of equilibrium statistical mechanics.

For ABPs, however, time reversal symmetry is explicitly broken. This can be seen directly from the overdamped Langevin equations:

$$\gamma \frac{d\mathbf{r}}{dt} = \gamma v_0 \mathbf{n}(t) - \nabla U(\mathbf{r}) + \xi(t)$$

$$\frac{d\theta}{dt} = \eta(t)$$

Under time reversal  $t \rightarrow -t$ , the position derivative transforms as  $\frac{d\mathbf{r}}{d(-t)} = -\frac{d\mathbf{r}}{dt}$ , meaning the left side of the equation changes sign. The random noise term  $\xi(-t)$  remains statistically equivalent to  $\xi(t)$  due to its time-symmetric properties. However, the self-propulsion term  $v_0 \mathbf{n}(t)$  behaves differently: while the orientation vector  $\mathbf{n}(t)$  would evolve backwards in time, the self-propulsion speed  $v_0$  maintains its sign because it represents an internal energy conversion process (chemical to mechanical) with a fixed directionality relative to the particle's orientation. This non-reversing active driving force is fundamentally different from reversible conservative forces, as it continually injects energy into the system. Consequently, the original equation and its time-reversed version describe physically distinct dynamics, demonstrating explicit time-reversal symmetry breaking in active systems.

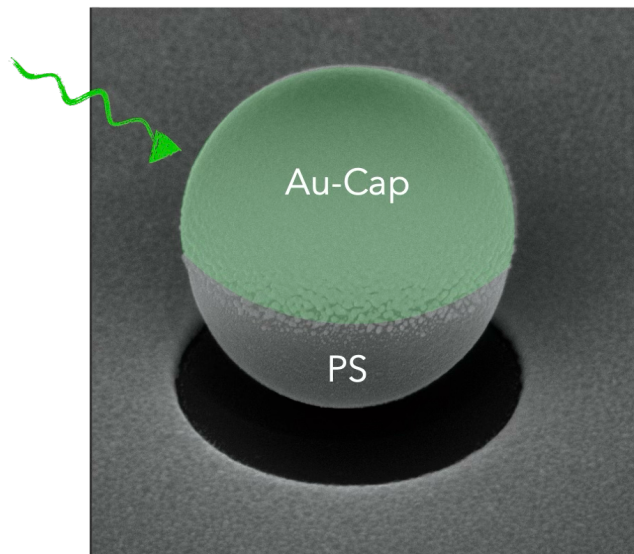


Figure 5.5: Janus particles exhibit physical asymmetry, with different properties on their two faces. This structural asymmetry leads to directional self-propulsion and breaking of time-reversal symmetry. The asymmetric design of Janus particles (e.g., with one catalytic hemisphere) creates directed motion that fundamentally breaks time-reversal symmetry. Under time reversal, the particle would appear to move against its catalytic face—a physically impossible scenario that illustrates the non-equilibrium nature of active particles.

Visually, this time-reversal asymmetry can be observed in trajectory data: forward trajectories show persistent motion along the instantaneous orientation, while time-reversed trajectories would appear to move persistently against their orientation—a scenario prohibited by the ABP dynamics. This persistence is also evident in the ballistic regime of the mean square displacement, which has no counterpart in equilibrium systems.

## FDT Violation

As we saw in Lecture 2, the fluctuation-dissipation theorem (FDT) connects the spontaneous fluctuations in equilibrium systems to their response to external perturbations. For ABPs, this theorem is violated due to the self-propulsion term that injects energy at the microscopic level.

The violation of the FDT can be quantified by introducing an effective temperature:

$$T_{\text{eff}} = T \left( 1 + \frac{v_0^2}{2D_t D_r} \right)$$

This effective temperature is higher than the bath temperature, reflecting the enhanced fluctuations due to activity.

## Taxonomy of Active Particle Models

Besides the two active particle models there are a number of other ones capturing different aspects of active motion.

Model	Key Characteristics	Movement Mechanism	Biological/Synthetic Examples	Physical Limitations
Run-and-Tumble Particles (RTPs)	Alternates between straight runs and random reorientations	Discrete reorientations at Poisson-distributed times	E. coli bacteria, Salmonella	Assumes instantaneous reorientations and ignores hydrodynamic interactions; real bacteria have finite tumbling durations and experience fluid resistance
Active Brownian Particles (ABPs)	Persistent propulsion with continuous rotational diffusion	Continuous rotational diffusion combined with constant propulsion speed	Janus colloids, synthetic microswimmers	Neglects hydrodynamic interactions and assumes constant propulsion regardless of environmental conditions; real swimmers may adjust speed based on energy constraints
Active Ornstein-Uhlenbeck Particles (AOUPs)	Self-propulsion with temporal correlations, Uhlenbeck colored noise	Velocity undergoes Ornstein-Uhlenbeck process with persistence time	Certain synthetic microswimmers, simplified model for biological cells	Lacks clear orientation-propulsion coupling present in real swimmers; statistical process may not accurately represent actual biological propulsion mechanisms

Model	Key Characteristics	Movement Mechanism	Biological/Synthetic Examples	Physical Limitations
Chiral Active Particles	Circular/helical trajectories due to intrinsic torque	Constant angular velocity combined with self-propulsion	Magnetotactic bacteria, sperm cells near surfaces	Assumes constant angular velocity and curvature radius; real organisms often modulate these parameters based on environmental cues and energetic constraints

## 5.4 Swimming at Low Reynolds Number

Microorganisms and synthetic microswimmers propel themselves in a liquid environment generally described by the Navier-Stokes equation, which governs fluid motion by balancing inertial forces with pressure gradients, viscous forces, and external forces:

$$\rho \left( \frac{\partial \mathbf{v}}{\partial t} + \mathbf{v} \cdot \nabla \mathbf{v} \right) = -\nabla p + \eta \nabla^2 \mathbf{v} + \mathbf{f}$$

Here,  $\rho$  is fluid density,  $\mathbf{v}$  is velocity,  $p$  is pressure,  $\eta$  is dynamic viscosity, and  $\mathbf{f}$  represents external force density. Through dimensional analysis, we can determine the relative importance of the inertial ( $\rho \mathbf{v} \cdot \nabla \mathbf{v}$ ) versus viscous ( $\eta \nabla^2 \mathbf{v}$ ) terms. If we scale length by  $L$ , velocity by  $V$ , and time by  $L/V$ , the inertial term scales as  $\rho V^2/L$  while the viscous term scales as  $\eta V/L^2$ . Their ratio yields the dimensionless Reynolds number:

$$Re = \frac{\rho v L}{\eta}$$

where  $\rho$  is the fluid density,  $v$  is the characteristic velocity,  $L$  is the characteristic length scale, and  $\eta$  is the fluid viscosity.

For a swimming bacterium like E. coli:

- $L \approx 1 \mu\text{m}$
- $v \approx 30 \mu\text{m/s}$
- $\rho \approx 10^3 \text{ kg/m}^3$  (water)
- $\eta \approx 10^{-3} \text{ Pa} \cdot \text{s}$  (water)

This gives  $Re \approx 3 \times 10^{-5}$ , indicating that viscous forces overwhelmingly dominate inertial forces. This regime presents unique challenges for locomotion that are fundamentally different from our macroscopic experience.

### The Scallop Theorem

At low Reynolds numbers, the inertial term in the Navier-Stokes equations can be dropped, leading to the simplified Stokes equations:

$$\eta \nabla^2 \mathbf{v} - \nabla p = 0$$

$$\nabla \cdot \mathbf{v} = 0$$

where  $\mathbf{v}$  is the fluid velocity and  $p$  is the pressure. These equations are linear and time-independent, which leads to the “scallop theorem”.

### The Scallop Theorem

The Scallop Theorem states that a microswimmer with a single degree of freedom cannot achieve net displacement in a Stokesian fluid (low Reynolds number). A scallop, which can only open and close its shell, represents such a mechanism with a single hinge. When the scallop opens slowly and closes rapidly in water, it generates thrust at the macroscale where inertia matters. However, at the microscale where viscous forces dominate, the time-reversibility of Stokes flow means the scallop would simply trace the same path backward and forward, resulting in no net movement regardless of how asymmetrically it times its opening and closing motions.

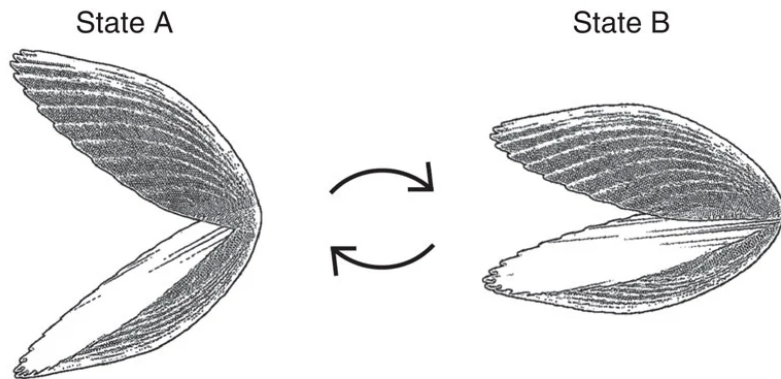


Figure 5.6: Illustration of the scallop theorem principle: a scallop-like mechanism with a single hinge can generate thrust at high Reynolds numbers (left) but produces no net motion at the microscale (right) where viscous forces dominate, as the motion is fully reversible. Source: [1] Yang, C., Liu, X., Song, X. & Zhang, L. Design and batch fabrication of anisotropic microparticles toward small-scale robots using microfluidics: recent advances. *Lab a Chip* 24, 4514–4535 (2024).

This theorem, formulated by Edward Purcell, can be understood as follows: if a swimmer changes its shape from A to B and then reverses this change from B to A along exactly the same path in configuration space, the net displacement will be zero. This is in stark contrast to swimming at high Reynolds numbers, where inertia allows for net displacement even with reciprocal motion.

### Breaking Time-Reversibility

To achieve net displacement at low Reynolds numbers, a swimmer must break time-reversibility. This can be done in several ways:

1. **Non-reciprocal deformation:** The swimmer changes shape in a way that is not simply the reverse of the previous motion. Examples include Purcell's three-link swimmer and the flexible oar.
2. **Chiral propellers:** Rotating a chiral structure like a bacterial flagellum creates propulsion. The helical shape of the flagellum converts rotational motion into translational thrust.
3. **Multiple degrees of freedom:** Using two or more degrees of freedom with phase differences between them (like the motion of cilia) creates non-reciprocal motion.

## 5.5 From Swimming to Hydrodynamic Interactions

When microorganisms swim at low Reynolds numbers, they don't just move themselves - they also generate flow fields in the surrounding fluid. These flow fields arise from the force-free swimming mechanisms we've explored and significantly influence how microswimmers interact with their environment and each other.

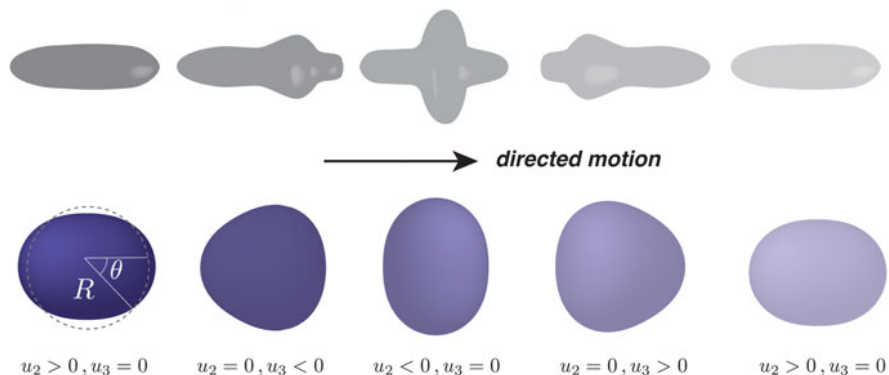


Figure 5.7: Amoeboid movement represents a classic example of non-reciprocal deformation, where the organism extends pseudopodia (temporary projections of cytoplasm) in a coordinated sequence that cannot be simply reversed. This asymmetric reshaping of the cell body enables locomotion even at low Reynolds numbers by creating a non-time-reversible sequence of configurations.

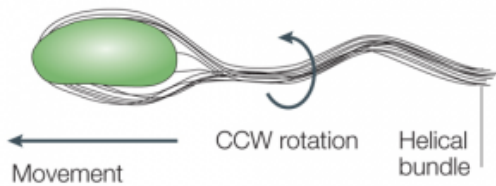


Figure 5.8: The helical structure of a bacterial flagellum allows it to convert rotational motion into translational thrust through a process known as the “whirlpool effect.” As the flagellum rotates, it creates a swirling motion in the surrounding fluid, which pushes the cell forward.

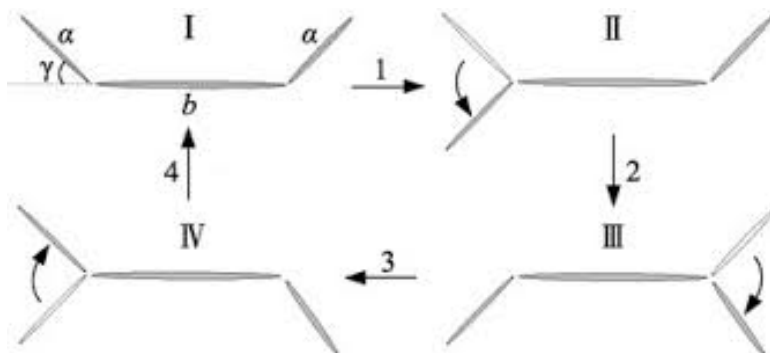


Figure 5.9: Purcell’s three-link swimmer demonstrates how a simple articulated structure with two degrees of freedom (two hinges) can achieve net displacement at low Reynolds numbers. By executing a non-reciprocal sequence of shape changes—moving the links in a way that cannot be reversed by simply retracing the path—this minimal swimmer breaks time-reversibility and generates directed motion in a viscous environment.

## The Origin of Hydrodynamic Singularities in Swimming

To understand how swimming generates flow fields, we need to examine two fundamental types of elementary flow patterns in Stokes flow:

1. **Source/sink dipoles:** These represent the displacement of fluid as a body moves through it. Consider a sphere moving through fluid - it pushes fluid ahead (source) and creates a region behind where fluid flows in (sink). These source dipoles:

- Decay rapidly with distance as  $1/r^3$
- Contribute to the propulsion of the swimmer
- Result from the swimmer's shape changes and boundary motion

The flow field generated by a source dipole with dipole moment  $\mathbf{p}$  at a position  $\mathbf{r}$  relative to the dipole center is:

$$\mathbf{u}_{\text{dipole}}(\mathbf{r}) = -\frac{1}{4\pi} \nabla \left( \frac{\mathbf{p} \cdot \mathbf{r}}{r^3} \right) = \frac{1}{4\pi} \left[ \frac{3(\mathbf{p} \cdot \mathbf{r})\mathbf{r}}{r^5} - \frac{\mathbf{p}}{r^3} \right]$$

where  $r = |\mathbf{r}|$ . This is analogous to the electric field of an electric dipole, with the  $1/r^3$  decay characteristic of dipole fields.

```
# Set up a grid
x = np.linspace(-3, 3, 100)
y = np.linspace(-3, 3, 100)
X, Y = np.meshgrid(x, y)

# Calculate R (distance from origin) for each point
R = np.sqrt(X**2 + Y**2)

# Define dipole moment vector (along x-axis)
p_x, p_y = 1.0, 0.0

# Calculate dot product p·r
p_dot_r = p_x*X + p_y*Y

# Set up arrays for velocity field components
u = np.zeros_like(X)
v = np.zeros_like(Y)

# Apply the dipole equation at each point where R > 0
# u = (1/4)[(3(p·r)x/r^5) - (p_x/r^3)]
# v = (1/4)[(3(p·r)y/r^5) - (p_y/r^3)]

mask = R > 0.2 # Avoid singularity at origin

u[mask] = (1/(4*np.pi))*(3*p_dot_r[mask]*X[mask]/R[mask]**5 - p_x/R[mask]**3)
v[mask] = (1/(4*np.pi))*(3*p_dot_r[mask]*Y[mask]/R[mask]**5 - p_y/R[mask]**3)

# Create plot
plt.figure(figsize=get_size(8, 8))

# Plot streamlines
plt.streamplot(X, Y, u, v, density=1, color='k', linewidth=1, arrowsize=0.5)

# Add dipole location and moment direction
plt.scatter(0, 0, color='red', s=50, label='Dipole location')
plt.arrow(0, 0, p_x*0.5, p_y*0.5, width=0.05, head_width=0.15,
```

```

head_length=0.2, fc='red', ec='red', label='Dipole moment')

plt.xlabel('x')
plt.ylabel('y')
plt.title('Source Dipole Flow Field')
plt.axis('equal')
plt.grid(True, linestyle='--', alpha=0.7)
plt.xlim(-3, 3)
plt.ylim(-3, 3)

plt.tight_layout()
plt.show()

```

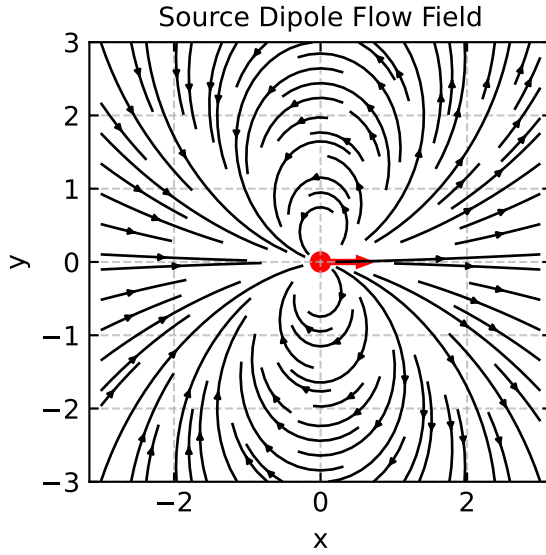


Figure 5.10: Flow field generated by a source dipole with dipole moment  $\mathbf{p}$  pointing in the x-direction. The streamlines show the characteristic pattern of fluid being pushed away along the dipole axis and drawn in from the sides, with the flow strength decaying as  $1/r^3$ .

2. **Force dipoles:** Since microswimmers are force-free (no net external force), the thrust forces they generate must be balanced by drag forces, creating a force dipole configuration. A force dipole is generated by two equal and opposite point forces aligned parallel to the x-axis, either both pointing towards the origin (converging) or both pointing away from the origin (diverging). These force dipoles:

- Decay more slowly with distance as  $1/r^2$
- Dominate the long-range hydrodynamic interactions
- Allow us to classify swimmers as either “pushers” (forces pointing away from the origin, like E. coli) or “pullers” (forces pointing towards the origin, like Chlamydomonas)

For a force dipole aligned along unit vector  $\mathbf{e}$ , the flow field is:

$$\mathbf{u}_{\text{stresslet}}(\mathbf{r}) = \frac{S}{8\pi\eta} \left[ \frac{3(\mathbf{e} \cdot \mathbf{r})^2 \mathbf{r} - r^2 \mathbf{e}}{r^5} \right]$$

where  $S$  is the stresslet strength (dipole moment) and  $\eta$  is the fluid viscosity. The sign of  $S$  determines the swimmer type:  $S < 0$  for pushers and  $S > 0$  for pullers. For a swimmer of size  $a$  moving at speed  $v_0$ , we can estimate  $S \sim \eta a^2 v_0$ .

At large distances, this simplifies to:

$$\mathbf{u}_{\text{stresslet}}(\mathbf{r}) \approx \frac{S}{8\pi\eta} \frac{3(\mathbf{e} \cdot \hat{\mathbf{r}})^2 - 1}{r^2} \hat{\mathbf{r}} \quad \text{as } r \rightarrow \infty$$

where  $\hat{\mathbf{r}} = \mathbf{r}/r$  is the direction vector.

```
# Create figure with two subplots for pusher and puller
fig, (ax1, ax2) = plt.subplots(1, 2, figsize=get_size(12, 6))

# Set up a grid
x = np.linspace(-3, 3, 100)
y = np.linspace(-3, 3, 100)
X, Y = np.meshgrid(x, y)

# Calculate R (distance from origin) for each point
R = np.sqrt(X**2 + Y**2)

# For both pusher and puller
for ax, S, title in zip([ax1, ax2], [-1.0, 1.0], ["Puller (S < 0)", "Pusher (S > 0)"]):
    # Set up arrays for velocity field components
    u = np.zeros_like(X)
    v = np.zeros_like(Y)

    # Avoid singularity at origin
    mask = R > 0.2
    eta = 1.0 # Normalize viscosity
    r_sq = X[mask]**2 + Y[mask]**2

    # x-component
    u[mask] = (S/(8*np.pi*eta)) * (3*(X[mask]**2)*X[mask] - r_sq*X[mask])/R[mask]**5

    # y-component
    v[mask] = (S/(8*np.pi*eta)) * (3*(X[mask]**2)*Y[mask] - 0)/R[mask]**5

    # Plot streamlines
    ax.streamplot(X, Y, u, v, density=1.2, color='k', linewidth=0.5, arrowsize=0.5)

    # Add force locations and arrows to visualize the dipole
    if S < 0: # Puller: forces pointing outward
        ax.arrow(-0.4, 0, 0.3, 0, width=0.05, head_width=0.15,
                  head_length=0.2, fc='red', ec='red')
        ax.arrow(0.4, 0, -0.3, 0, width=0.05, head_width=0.15,
                  head_length=0.2, fc='red', ec='red')
        ax.scatter([-0.4, 0.4], [0, 0], color='red', s=50)
    else: # Pusher: forces pointing inward
        ax.arrow(-0.4, 0, -0.3, 0, width=0.05, head_width=0.15,
                  head_length=0.2, fc='red', ec='red')
        ax.arrow(0.4, 0, 0.3, 0, width=0.05, head_width=0.15,
                  head_length=0.2, fc='red', ec='red')
        ax.scatter([-0.4, 0.4], [0, 0], color='red', s=50)

    ax.set_xlabel('x')
    ax.set_ylabel('y')
    ax.set_title(title)
    ax.set_xlim(-3, 3)
    ax.set_ylim(-3, 3)
    ax.set_aspect('equal')
```

```

ax.grid(True, linestyle='--', alpha=0.7)

plt.tight_layout()
plt.show()

```

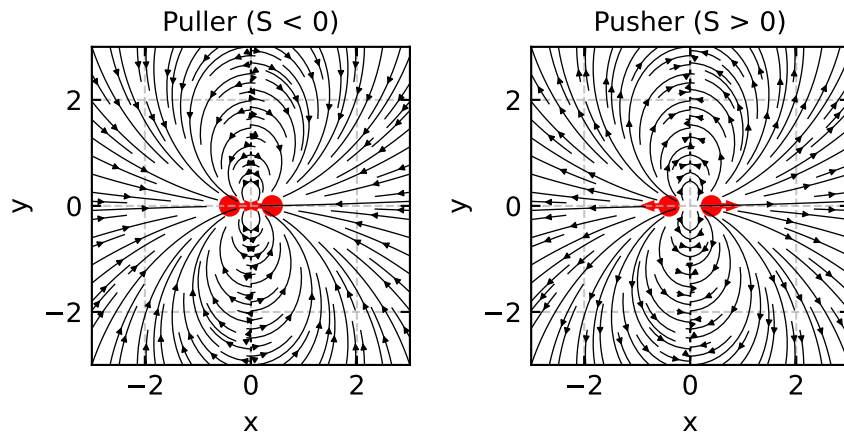


Figure 5.11: Pusher Puller

In the far field, the flow generated by a force dipole (pusher,  $S > 0$ ) at large distances from the swimmer exhibits a dominant  $1/r^2$  decay pattern. Fluid is pulled in from the sides and pushed away along the swimming direction.

```

# Set up a grid for far-field visualization (larger domain)
x_far = np.linspace(-10, 10, 100)
y_far = np.linspace(-10, 10, 100)
X_far, Y_far = np.meshgrid(x_far, y_far)

# Calculate R (distance from origin) for each point
R_far = np.sqrt(X_far**2 + Y_far**2)

# Set up arrays for velocity field components
u_far = np.zeros_like(X_far)
v_far = np.zeros_like(Y_far)

# Parameters
S = 1.0 # Positive for pusher
eta = 1.0 # Normalized viscosity
e_x, e_y = 1.0, 0.0 # Unit vector along x-axis

# Avoid singularity at origin
mask_far = R_far > 0.5

# Compute unit radial vectors
r_hat_x = X_far[mask_far] / R_far[mask_far]
r_hat_y = Y_far[mask_far] / R_far[mask_far]

# Compute e·r̂
e_dot_r_hat = e_x*r_hat_x + e_y*r_hat_y

# Far-field approximation: u = (S/8) [(3(e·r̂)^2 - 1)/r^2] r̂
# Calculate the scalar coefficient

```

```
coef = (S/(8*np.pi*eta)) * (3*e_dot_r_hat**2 - 1) / R_far[mask_far]**2

# Apply to get velocity components
u_far[mask_far] = coef * r_hat_x
v_far[mask_far] = coef * r_hat_y

# Create plot
plt.figure(figsize=get_size(10, 8))

# Plot streamlines for far-field approximation
plt.streamplot(X_far, Y_far, u_far, v_far, density=1.0, color='k',
                linewidth=0.8, arrowsize=0.8)

# Add swimming direction indication
plt.arrow(0, 0, 2, 0, width=0.2, head_width=0.6,
          head_length=0.8, fc='blue', ec='blue', alpha=0.7)
plt.scatter(0, 0, color='blue', s=80, alpha=0.7, label='Swimmer')

plt.xlabel('x')
plt.ylabel('y')
plt.title('Far-field Force Dipole Flow (Pusher)')
plt.axis('square')
plt.xlim(-10, 10)
plt.ylim(-10, 10)

# Add a circle to indicate the near-field region
circle = plt.Circle((0, 0), 2, fill=False, color='red', linestyle='--', alpha=0.7)
plt.gca().add_patch(circle)
plt.text(2.2, 0.5, 'Near-field', color='red', alpha=0.7)

plt.tight_layout()
plt.show()
```

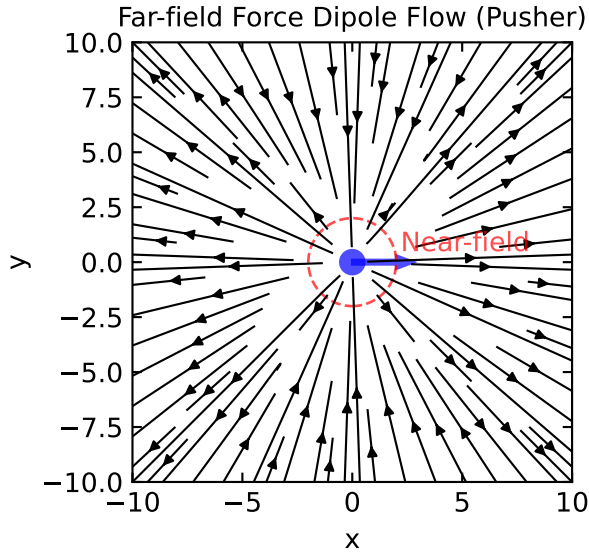


Figure 5.12: Far-field approximation of the flow generated by a force dipole (pusher,  $S > 0$ ) at large distances from the swimmer. The streamlines illustrate how the dominant  $1/r^2$  decay pattern emerges, with fluid being pulled in from the sides and pushed away along the swimming direction.

This distinction has important physical consequences: source dipoles enable self-propulsion but decay rapidly, while force dipoles dominate the long-range interactions between swimmers. These flow fields can be derived from the fundamental solution of Stokes flow (the Oseen tensor):

$$G_{ij}(\mathbf{r}) = \frac{1}{8\pi\eta} \left( \frac{\delta_{ij}}{r} + \frac{r_i r_j}{r^3} \right)$$

which gives the velocity field at position  $\mathbf{r}$  due to a point force at the origin.